Nonlinear vibrations and energy exchange of single-walled carbon nanotubes. Circumferential flexural modes

Matteo Strozzi[a], Valeri V. Smirnov[b], Leonid I. Manevitch[b],
Massimo Milani[a], Francesco Pellicano[c,*]

[a]Department of Sciences and Methods for Engineering, University of Modena and Reggio Emilia,
Via Giovanni Amendola 2, 42122 Reggio Emilia, Italy

[b]N.N. Semenov Institute of Chemical Physics, Russian Academy of Sciences RAS,
ulica Kosygina 4, 119991 Moscow, Russia

[c]Department of Engineering "Enzo Ferrari", University of Modena and Reggio Emilia,
Via Pietro Vivarelli 10/1, 41125 Modena, Italy

Running headline: Nonlinear vibrations and energy exchange of single-walled carbon nanotubes. Circumferential flexural modes

Number of Pages = 47
Number of Tables = 8
Number of Figures = 13

Dr. Francesco Pellicano, Professor
Department of Engineering "Enzo Ferrari"
University of Modena and Reggio Emilia
Via Pietro Vivarelli 10/1
41125 Modena, Italy
Phone: +39 059 205 6154
Fax: +39 059 205 6126
email: francesco.pellicano@unimore.it

Abstract

In this paper, the nonlinear vibrations and energy exchange of single-walled carbon nanotubes (SWNTs) are studied. The Sanders-Koiter theory is applied to model the nonlinear dynamics of the system in the case of finite amplitude of vibration. The SWNT deformation is described in terms of longitudinal, circumferential and radial displacement fields. Simply supported, clamped and free boundary conditions are considered. The circumferential flexural modes (CFMs) are investigated. Two different approaches based on numerical and analytical models are compared. In the numerical model, an energy method based on the Lagrange equations is used to reduce the nonlinear partial differential equations of motion to a set of nonlinear ordinary differential equations, which is solved by using the implicit Runge-Kutta numerical method. In the analytical model, a reduced form of the Sanders-Koiter theory assuming small circumferential and tangential shear deformations is used to get the nonlinear ordinary differential equations of motion, which are solved by using the multiple scales analytical method. The transition from energy beating to energy localization in the nonlinear field is studied. The effect of the aspect ratio on the analytical and numerical values of the nonlinear energy localization threshold for different boundary conditions is investigated.

Keywords

Carbon nanotubes; nonlinear vibrations; energy localization; circumferential flexural modes

1. Introduction

In this paper, we are going to study the problems of the energy exchange and localization along the SWNT axis by considering appropriate parameters and models, where the energy transfer denotes a strongly non-stationary and resonant nonlinear dynamic process.

The spatially localized excitations represent one of the most interesting phenomena in the nonlinear dynamics of solids and structures [1]. In particular, the spatial confinement of nonlinear vibrations generated by external loads can be used to develop robust shock and vibration isolation designs for certain classes of engineering systems [2]. Moreover, excitations of this type determine elementary mechanisms of many physical processes giving noticeable contributions to thermal conductivity [3].

In the cases of discrete structures, the nonlinear dynamic processes can be studied in the framework of Nonlinear Normal Modes (NNMs) or Limiting Phase Trajectories (LPTs).

The NNMs are usually applied in order to describe stationary and non-stationary, but non-resonant, nonlinear dynamic processes; therefore, they are not involved into energy exchange and localization problems, which are strongly non-stationary and resonant nonlinear dynamic processes.

Conversely, the LPTs are applied to model strongly non-stationary and resonant nonlinear dynamic processes, such as energy exchange and localization, describing the maximum possible (under given conditions) nonlinear energy transfer between different parts of the considered system.

Manevitch and Musienko [4] presented an analytical description of transient vibrations of a forced an-harmonic oscillator. They used the LPTs to describe the intensive energy exchange which causes two dynamical transitions by increasing the amplitude of the nonlinearity parameter.

Manevitch et al. [5] considered the nonlinear energy exchange of two coupled oscillators subjected to a 1:1 resonance by means of the LPTs. They demonstrated that the most intense energy exchange arises when the motion of the equivalent single oscillator is close to the LPTs.

Manevitch and Smirnov [6] described the energy exchange and transition to energy localization in the finite periodic Fermi-Pasta-Ulam nonlinear oscillatory chain in terms of effective particles and LPTs. They calculated the excitation level corresponding to non-stationary energy localizations.

Smirnov and Manevitch [7] studied the strong energy exchange between different parts of periodic nonlinear Frenkel-Kontorova and Klein-Gordon lattices by considering the LPTs assumption. They developed an asymptotic analysis to obtain the values of the dynamic energy transitions.

Since, in this paper, we are going to consider the strongly non-stationary, resonant dynamic process of the energy transfer along the SWNT axis, then the LPTs (and not the NNMs) will be considered.

The concepts of effective particles and limiting phase trajectories have been extended also to the SWNTs, which are finite discrete carbon structures consisting of needle-like microtubules [8].

Smirnov et al. [9] studied the localization of bending vibrations in SWNTs in terms of LPTs. They analysed the intensive resonant interaction of zone-boundary and nearest modes leading to loss of stability and effective confinement of the energy in one part of the system (localization threshold).

Smirnov et al. [10] considered the energy exchange and localization in SWNTs for circumferential flexural oscillations. The origin of weak energy localization was clarified by means of LPTs. The analytical results were confirmed by comparisons with numerical approach and MD simulations.

Because of their nanoscale size, it is very difficult to investigate the mechanical properties of the nanotubes by using experimental techniques, which require the use of high-resolution transmission electron microscopes. On the other hand, it was found that molecular dynamics (MD) simulations provide good predictions of the mechanical behaviour of CNTs under external forces, with results close to the experiments [11].

The analogies between the continuous shells and the discrete SWNTs led to a very large application of the elastic shell theories for the SWNT structural analysis.

Liew and Wang [12] investigated the wave propagation in SWNTs via two different elastic shell theories, i.e., Love's thin cylindrical shell theory and Cooper-Naghdi thick cylindrical shell theory, the last one taking into account also the shear and inertia effects.

Wang et al. [13] studied static buckling and free vibrations of simply supported SWNTs comparing the results of the Donnell shallow shell theory and the simplified Flugge thin shell theory with the results of the exact Flugge thin shell theory, which retains all the three displacement fields.

Silvestre [14] investigated the buckling behaviour of clamped SWNTs under external torsion using the Donnell shallow shell theory and the Sanders-Koiter thin shell theory in a wide range of aspect ratios, diameters and chiralities.

Hu et al. [15] investigated the transverse and torsional wave propagations in SWNTs by comparing the results of a nonlocal elastic shell model based on the Eringen's parameter and the results of the classical Donnell and Sanders thin shell theories.

Silvestre et al. [16] used the Donnell shallow shell and Sanders-Koiter thin shell theories to study the buckling behaviour and relative mode shapes of axially compressed simply supported SWNTs presenting a small aspect ratio.

Strozzi et al. [17] studied the low-frequency linear vibrations of SWNTs in the framework of the Sanders-Koiter thin shell theory. Two approaches, based on numerical and analytical models, were compared. Several types of SWNTs were analysed by varying aspect ratio and chirality.

Other relevant studies on CNTs nonlinear vibrations and instability can be found in Refs. [18-28].

In this paper, the discrete SWNTs are modelled as continuum elastic thin circular cylindrical shells considering equivalent mechanical parameters, and the nonlinear dynamics of the SWNTs is studied

by considering the Sanders-Koiter nonlinear thin shell theory; it must be clearly pointed out that the present paper starts from the Sanders-Koiter linear shell theory and corresponding numerical results reported in Ref. [17], extending the theory and numerical results to the nonlinear field.

A deep dissertation on the nonlinear vibrations of cylindrical shells can be found in Refs. [29-32].

In particular, the effect of the boundary conditions on the nonlinear vibrations of circular cylindrical shells has been intensely investigated in the pertinent literature in the past years.

Kurylov and Amabili [33] studied the nonlinear vibrations of clamped-free cylindrical shells with geometric imperfection. The Sanders-Koiter shell theory was used to study the nonlinear dynamics. An energy approach based on Lagrange equations was applied to obtain the equations of motion.

Pellicano [34] investigated the nonlinear vibrations of cylindrical shells by means of the Sanders-Koiter shell theory. Simply supported and clamped boundary conditions were considered, as well as connections with rigid bodies; in the latter case, experiments were carried out.

Amabili [35] considered the nonlinear vibrations of cylindrical shells subjected to a radial harmonic excitation. Simply supported shells with allowed and constrained axial displacements at the edges were studied. The Donnell and Novozhilov thin shell theories were applied.

Zhang et al. [36] used the local adaptive differential quadrature method for the nonlinear vibrations study of simply supported, clamped and free cylindrical shells. The nonlinear equations of motion were formulated by means of the Goldenveizer-Novozhilov shell theory.

Kurylov and Amabili [37] studied the geometrical nonlinear forced vibrations of cylindrical shells by considering the Sanders-Koiter shell theory. Simply supported and clamped boundary conditions were investigated. The Lagrangian approach was applied to obtain the equations of motion.

Strozzi and Pellicano [38-39] analysed the nonlinear vibrations of functionally graded cylindrical shells for simply supported, clamped and free boundary conditions. The Sanders-Koiter shell theory was applied to describe the nonlinear dynamics of the shell subjected to a harmonic external load.

In the present paper, the nonlinear vibrations and energy exchange of SWNTs are investigated. The SWNT dynamics is studied within the framework of the Sanders-Koiter theory. The circumferential flexural modes (CFMs) are evaluated. The SWNT deformation is described in term of longitudinal, circumferential and radial displacement fields. Simply supported, clamped and free boundary conditions are examined. Two different approaches are proposed, based on numerical and analytical models. In the numerical model, the three displacement fields are expanded in nonlinear field by using approximate linear eigenfunctions. An energy method based on the Lagrange equations is used to reduce the nonlinear partial differential equations of motion to a set of nonlinear ordinary differential equations, which is solved by using the implicit Runge-Kutta numerical method. In the analytical model, a reduced form of the Sanders-Koiter theory assuming small circumferential and

tangential shear deformations is considered. A fourth-order nonlinear partial differential equation of motion for the radial displacement field is derived, which allows the effect of the nonlinearity for the different boundary conditions to be estimated. An analytical solution of this differential equation of motion is obtained applying the multiple scales method. In the second part of the present paper, the transition from energy beating to energy localization in the nonlinear field is investigated; the concept of energy localization is introduced, which represents a strongly nonlinear phenomenon.

In the case of small amplitude initial energy, a periodic energy exchange between the two halves of the nanotube takes place. The nonlinear oscillations of the SWNT become localized when the initial excitation intensity exceeds some energy threshold which depends on the length of the SWNT; the amplitude of the smallest initial excitation, corresponding to the energy confinement in one half of the nanotube axis, is called energy localization threshold. In this paper, the transition from energy beating to energy localization in SWNTs is investigated using numerical and analytical approaches, where the analytical approach is based on the LPTs concept. The effect of the SWNT aspect ratio on the analytical and numerical values of the energy localization threshold is investigated; different boundary conditions are evaluated.

2. Sanders-Koiter nonlinear shell theory

First of all, it is very important to underline that the present paper starts from the results obtained in the linear field reported in Ref. [17], and extends these analyses to the nonlinear field.

In Figure 1, a circular cylindrical shell having radius R, length L and thickness h is represented; a cylindrical coordinate system (O; x, θ, z) is considered where the origin O of the reference system is located at the centre of one end of the shell. In Figure 1, three displacement fields are represented: longitudinal u (x, θ, t), circumferential v (x, θ, t) and radial w (x, θ, t); the radial displacement field w is considered positive outward; (x, θ) are the longitudinal and angular coordinates of an arbitrary point on the middle surface of the shell; z is the radial coordinate along the thickness h; t is the time.

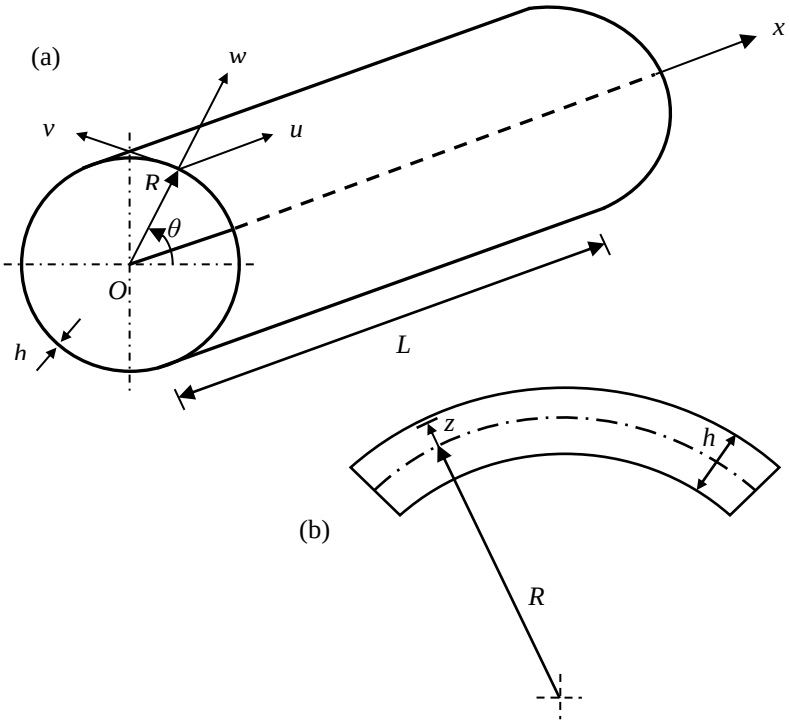

Figure 1. Geometry of the circular cylindrical shell.
(a) Complete shell; (b) cross-section of the shell surface.

2.1. Displacement fields and strain-displacement relationships

The nondimensional displacement fields $(\tilde{u}, \tilde{v}, \tilde{w})$ can be written in the following form [17]

$$\tilde{u} = \frac{u}{R} \qquad \tilde{v} = \frac{v}{R} \qquad \tilde{w} = \frac{w}{R} \tag{1}$$

where (u,v,w) are the dimensional displacement fields and R is the radius of the carbon nanotube.

The nondimensional middle surface strains of the shell $(\tilde{\varepsilon}_{x,0}, \tilde{\varepsilon}_{\theta,0}, \tilde{\gamma}_{x\theta,0})$ are expressed as [38]

$$\tilde{\varepsilon}_{x,0} = \alpha \frac{\partial \tilde{u}}{\partial \eta} + \frac{1}{2}\alpha^2 \left(\frac{\partial \tilde{w}}{\partial \eta}\right)^2 + \frac{1}{8}\left(\alpha \frac{\partial \tilde{v}}{\partial \eta} - \frac{\partial \tilde{u}}{\partial \theta}\right)^2 \tag{2}$$

$$\tilde{\varepsilon}_{\theta,0} = \frac{\partial \tilde{v}}{\partial \theta} + \tilde{w} + \frac{1}{2}\left(\frac{\partial \tilde{w}}{\partial \theta} - \tilde{v}\right)^2 + \frac{1}{8}\left(\frac{\partial \tilde{u}}{\partial \theta} - \alpha \frac{\partial \tilde{v}}{\partial \eta}\right)^2 \tag{3}$$

$$\tilde{\gamma}_{x\theta,0} = \frac{\partial \tilde{u}}{\partial \theta} + \alpha \frac{\partial \tilde{v}}{\partial \eta} + \alpha \frac{\partial \tilde{w}}{\partial \eta}\left(\frac{\partial \tilde{w}}{\partial \theta} - \tilde{v}\right) \tag{4}$$

where $\eta = x/L$ is the nondimensional longitudinal coordinate of the shell and $\alpha = R/L$.

The nondimensional middle surface changes in curvature and torsion of the shell $(\tilde{k}_x, \tilde{k}_\theta, \tilde{k}_{x\theta})$ are given by [17]

$$\tilde{k}_x = -\alpha^2 \frac{\partial^2 \tilde{w}}{\partial \eta^2} \qquad \tilde{k}_\theta = \frac{\partial \tilde{v}}{\partial \theta} - \frac{\partial^2 \tilde{w}}{\partial \theta^2} \qquad \tilde{k}_{x\theta} = -2\alpha \frac{\partial^2 \tilde{w}}{\partial \eta \partial \theta} + \frac{3}{2}\alpha \frac{\partial \tilde{v}}{\partial \eta} - \frac{1}{2}\frac{\partial \tilde{u}}{\partial \theta} \tag{5}$$

It should be underlined that in equations (2)-(3)-(4) the nonlinear terms are considered, while they are neglected in equation (5). According to the Sanders-Koiter nonlinear shell theory, the middle surface strains (equations 2-4) contain both linear and nonlinear terms, while the middle surface changes in curvature and torsion (equation 5) are linear [31]. On the other hand, according to the Novozhilov and Flugge-Lur'e-Byrne nonlinear shell theories, the nonlinear terms in changes in curvature and torsion are retained [31]. It was demonstrated that numerical results for the nonlinear vibrations obtained by Sanders-Koiter, Flugge-Lur'e-Byrne and Novozhilov nonlinear shell theories in the specific case of thin shells (as investigated in the present paper) are extremely close, see Ref. [32] for more details.

2.2. Force and moment resultants

The nondimensional force ($\tilde{N}_x, \tilde{N}_\theta, \tilde{N}_{x\theta}, \tilde{Q}_x, \tilde{Q}_\theta$) and moment ($\tilde{M}_x, \tilde{M}_\theta, \tilde{M}_{x\theta}$) resultants are written in the following form [17]

$$\tilde{N}_x = \tilde{\varepsilon}_{x,0} + \nu \tilde{\varepsilon}_{\theta,0} \qquad \tilde{N}_\theta = \tilde{\varepsilon}_{\theta,0} + \nu \tilde{\varepsilon}_{x,0} \qquad \tilde{N}_{x\theta} = \frac{(1-\nu)}{2}\tilde{\gamma}_{x\theta,0}$$

$$\tilde{Q}_x = \alpha(\tilde{k}_{x,x} + \nu\tilde{k}_{\theta,x}) + \frac{(1-\nu)}{2}\tilde{k}_{\theta x,\theta} \qquad \tilde{Q}_\theta = \alpha\frac{(1-\nu)}{2}\tilde{k}_{x\theta,x} + \tilde{k}_{\theta,\theta} + \nu\tilde{k}_{x,\theta} \tag{6}$$

$$\tilde{M}_x = \tilde{k}_x + \nu\tilde{k}_\theta \qquad \tilde{M}_\theta = \tilde{k}_\theta + \nu\tilde{k}_x \qquad \tilde{M}_{x\theta} = \frac{(1-\nu)}{2}\tilde{k}_{x\theta}$$

2.3. Elastic strain energy

The nondimensional elastic strain energy $\tilde{E}$ of a cylindrical shell is expressed as follows [17]

$$\tilde{E} = \frac{1}{2}\frac{1}{(1-\nu^2)}\left\{\int_0^1\int_0^{2\pi}\left[\tilde{\varepsilon}_{x,0}^2 + \tilde{\varepsilon}_{\theta,0}^2 + 2\nu\tilde{\varepsilon}_{x,0}\tilde{\varepsilon}_{\theta,0} + \frac{(1-\nu)}{2}\tilde{\gamma}_{x\theta,0}^2\right]d\eta d\theta + \frac{\beta^2}{12}\int_0^1\int_0^{2\pi}\left[\tilde{k}_x^2 + \tilde{k}_\theta^2 + 2\nu\tilde{k}_x\tilde{k}_\theta + \frac{(1-\nu)}{2}\tilde{k}_{x\theta}^2\right]d\eta d\theta\right\} \tag{7}$$

where the first term of the right-hand side of equation (7) is the membrane energy (also referred to stretching energy) and the second one is the bending energy, with $\beta = h/R$.

2.4. Kinetic energy

The nondimensional time variable τ can be defined by introducing a reference circular frequency ω_0 in the form [17]

$$\tau = \omega_0 t \qquad \omega_0 = \sqrt{\frac{E}{(1-\nu^2)\rho R^2}} \tag{8}$$

where t is the dimensional time variable and (E, ν, ρ) are the Young's modulus, Poisson's ratio and mass density of the cylindrical shell.

The nondimensional velocity fields $(\tilde{u}', \tilde{v}', \tilde{w}')$ can be obtained from the dimensional displacement fields $(\tilde{u}, \tilde{v}, \tilde{w})$ and the nondimensional time τ in the following form [17]

$$\tilde{u}' = \frac{d\tilde{u}}{d\tau} \qquad \tilde{v}' = \frac{d\tilde{v}}{d\tau} \qquad \tilde{w}' = \frac{d\tilde{w}}{d\tau} \tag{9}$$

The nondimensional kinetic energy $\tilde{T}$ of a cylindrical shell is given by [17]

$$\tilde{T} = \frac{1}{2}\gamma \int_0^1 \int_0^{2\pi} (\tilde{u}'^2 + \tilde{v}'^2 + \tilde{w}'^2) d\eta d\theta \tag{10}$$

where $\gamma = \rho R^2 \omega_0^2 / E$.

3. Numerical solution of the Sanders-Koiter nonlinear shell theory

In order to obtain a numerical solution of the SWNT nonlinear dynamics, a two-steps procedure is considered: i) the three displacement fields are expanded by using the approximated eigenfunctions obtained in linear field; ii) the Lagrange equations are considered in conjunction with the nonlinear elastic strain energy in order to obtain a set of nonlinear ordinary differential equations of motion.
The linear vibration analysis is reported in detail in Ref. [17].

3.1. Nonlinear vibration analysis

In the nonlinear vibration analysis, the full expression of the nondimensional elastic strain energy $\tilde{E}$ (7), which contains terms up to the fourth order (cubic nonlinearity), is considered.
The three displacement fields $\tilde{u}(\eta,\theta,\tau)$, $\tilde{v}(\eta,\theta,\tau)$, $\tilde{w}(\eta,\theta,\tau)$ are expanded using the mode shapes $\tilde{U}^{(j,n)}(\eta,\theta)$, $\tilde{V}^{(j,n)}(\eta,\theta)$, $\tilde{W}^{(j,n)}(\eta,\theta)$ obtained in the linear vibration analysis, in the form [38]

$$\begin{aligned}
\tilde{u}(\eta,\theta,\tau) &= \sum_{j=1}^{N_u}\sum_{n=1}^{N}\tilde{U}^{(j,n)}(\eta,\theta)\,\tilde{f}_{u,j,n}(\tau)\\
\tilde{v}(\eta,\theta,\tau) &= \sum_{j=1}^{N_v}\sum_{n=1}^{N}\tilde{V}^{(j,n)}(\eta,\theta)\,\tilde{f}_{v,j,n}(\tau)\\
\tilde{w}(\eta,\theta,\tau) &= \sum_{j=1}^{N_w}\sum_{n=1}^{N}\tilde{W}^{(j,n)}(\eta,\theta)\,\tilde{f}_{w,j,n}(\tau)
\end{aligned} \tag{11}$$

where the time laws $(\tilde{f}_{u,j,n}(\tau), \tilde{f}_{v,j,n}(\tau), \tilde{f}_{w,j,n}(\tau))$ are unknown functions (step i).
The mode shapes $\tilde{U}^{(j,n)}(\eta,\theta)$, $\tilde{V}^{(j,n)}(\eta,\theta)$, $\tilde{W}^{(j,n)}(\eta,\theta)$ are known functions expressed in terms of Chebyshev polynomials and harmonic functions [17], where the index *j* is used for ordering the modes with increasing associated natural frequency and the index *n* indicates the number of nodal diameters; since these mode shapes respect exactly the boundary conditions, then also expansions (11) respect exactly the boundary conditions.
Moreover, the time synchronicity is now relaxed since for each mode *j* and for each component $(\tilde{u},\tilde{v},\tilde{w})$ different time laws $\tilde{f}(\tau)$ are allowed (the linear modes are now decoupled by considering the nonlinear time laws).

3.2. Lagrange equations

Expansions (11) are inserted into the expressions of elastic strain energy $\tilde{E}$ (7) and kinetic energy $\tilde{T}$ (10); then, the nondimensional Lagrange equations of motion for free vibrations can be expressed in the form

$$\frac{d}{d\tau}\left(\frac{\partial \tilde{T}}{\partial \tilde{q}_i^{'}}\right)+\frac{\partial \tilde{E}}{\partial \tilde{q}_i}=0 \qquad i\in[1,N_{\max}] \qquad (12)$$

where the maximum number of degrees of freedom $N_{\max}$ depends on the number of vibration modes considered in the expansions (11).

The nondimensional lagrangian coordinates $(\tilde{q}_i,\tilde{q}_i^{'})$ can be written as

$$\tilde{q}_i=\frac{q_i}{R} \qquad \tilde{q}_i^{'}=\frac{d\tilde{q}_i}{d\tau} \qquad i\in[1,N_{\max}] \qquad (13)$$

where the nondimensional lagrangian coordinates $\tilde{q}_i$ correspond to the previous nondimensional modal coordinates $(\tilde{f}_{u,j,n}(\tau),\tilde{f}_{v,j,n}(\tau),\tilde{f}_{w,j,n}(\tau))$.

By substituting the vector functions $\tilde{F}(\tilde{q}_i)=\partial\tilde{E}/\partial\tilde{q}_i$ and $\tilde{M}\tilde{q}_i^{''}=d(\partial\tilde{T}/\partial\tilde{q}_i^{'})/d\tau$ into equation (12), where $\tilde{M}$ denotes the mass matrix, we obtain

$$\tilde{M}\tilde{q}_i^{''}+\tilde{F}(\tilde{q}_i)=0 \qquad i\in[1,N_{\max}] \qquad (14)$$

Introducing the vector function $\tilde{F}_{x,i}=\tilde{M}^{-1}\tilde{F}(\tilde{q}_i)$ in the equation (14), the nondimensional Lagrange equations of motion for free vibrations can be expressed in the following form

$$\tilde{q}_i^{''}+\tilde{F}_{x,i}=0 \qquad i\in[1,N_{\max}] \qquad (15)$$

Using the Lagrange equations (15), a set of nonlinear ordinary differential equations is obtained; these equations must be completed with suitable modal initial conditions on the displacements and velocities (step ii). This system of nonlinear equations of motion is solved numerically by using the implicit Runge-Kutta method with suitable accuracy, precision and number of steps.

4. Analytical solution of the Sanders-Koiter nonlinear shell theory

In order to obtain an analytical solution of the SWNT nonlinear dynamics, a two-steps procedure is considered: i) a reduced form of the Sanders-Koiter nonlinear theory is developed, and a nonlinear partial differential equation of motion is obtained for the radial displacement field; ii) the Galerkin method is considered in order to obtain a set of nonlinear ordinary differential equations of motion. The linear vibration analysis is reported in detail in Ref. [17].

4.1. Nonlinear vibration analysis

In the present section, the reduced form of the Sanders-Koiter linear shell theory developed in Ref. [17] is extended to the nonlinear field. The nonlinear expansions of the nondimensional longitudinal $\tilde{u}$, circumferential $\tilde{v}$ and radial $\tilde{w}$ displacement fields can be written as [17]

$$\begin{aligned} \tilde{u}(\eta,\theta,\tau) &= \tilde{U}_0(\eta,\tau) + \tilde{U}(\eta,\tau)\cos(n\theta) \\ \tilde{v}(\eta,\theta,\tau) &= \tilde{V}(\eta,\tau)\sin(n\theta) \\ \tilde{w}(\eta,\theta,\tau) &= \tilde{W}_0(\eta,\tau) + \tilde{W}(\eta,\tau)\cos(n\theta) \end{aligned} \tag{16}$$

where $\tilde{U}_0$ and $\tilde{W}_0$ describe the axisymmetric component of the longitudinal and radial displacement. By neglecting the nondimensional middle surface circumferential normal strain of equation (3)

$$\tilde{\varepsilon}_{\theta,0} = \frac{\partial \tilde{v}}{\partial \theta} + \tilde{w} + \frac{1}{2}\left(\frac{\partial \tilde{w}}{\partial \theta} - \tilde{v}\right)^2 + \frac{1}{8}\left(\frac{\partial \tilde{u}}{\partial \theta} - \alpha\frac{\partial \tilde{v}}{\partial \eta}\right)^2 = 0 \tag{17}$$

and the nondimensional middle surface tangential shear strain of equation (4)

$$\tilde{\gamma}_{x\theta,0} = \frac{\partial \tilde{u}}{\partial \theta} + \alpha\frac{\partial \tilde{v}}{\partial \eta} + \alpha\frac{\partial \tilde{w}}{\partial \eta}\left(\frac{\partial \tilde{w}}{\partial \theta} - \tilde{v}\right) = 0 \tag{18}$$

the nondimensional longitudinal and circumferential displacement fields can be written as functions of the nondimensional radial displacement field in the following form

$$\tilde{V}(\eta,\tau)=-\frac{1}{n}\tilde{W}(\eta,\tau) \qquad \tilde{U}(\eta,\tau)=-\frac{\alpha}{n^2}\frac{\partial\tilde{W}(\eta,\tau)}{\partial\eta}$$

$$\frac{\partial\tilde{U}_0(\eta,\tau)}{\partial\eta}=-\frac{\alpha(n^2+1)}{4n^2}\left(\frac{\partial\tilde{W}(\eta,\tau)}{\partial\eta}\right)^2 \quad \tilde{W}_0(\eta,\tau)=-\frac{1}{4n^2}\left[(n^2-1)^2\tilde{W}^2(\eta,\tau)+\alpha^2\left(\frac{\partial\tilde{W}(\eta,\tau)}{\partial\eta}\right)^2\right] \tag{19}$$

and the nonlinear partial differential equation of motion for the nondimensional radial displacement field $\tilde{W}(\eta,\tau)$ is written in the following form (step i)

$$\begin{aligned}&\frac{\partial^2\tilde{W}}{\partial\tau^2}+\frac{\beta^2n^2(n^2-1)^2}{12(n^2+1)}\tilde{W}-\frac{\alpha^2\beta^2(n^2-1)(n^2-1+\nu)}{6(n^2+1)}\frac{\partial^2\tilde{W}}{\partial\eta^2}-\frac{\alpha^2}{n^2(n^2+1)}\frac{\partial^4\tilde{W}}{\partial\eta^2\partial\tau^2}+\\&\frac{\alpha^4(12+n^4\beta^2)}{12n^2(n^2+1)}\frac{\partial^4\tilde{W}}{\partial\eta^4}+\frac{(n^2-1)^4}{2n^2(n^2+1)}\tilde{W}\left[\left(\frac{\partial\tilde{W}}{\partial\tau}\right)^2+\tilde{W}\frac{\partial^2\tilde{W}}{\partial\tau^2}\right]+\frac{2\alpha^4(n^2-1)^2}{n^2(n^2+1)}\left(\frac{\partial\tilde{W}}{\partial\eta}\right)^2\frac{\partial^2\tilde{W}}{\partial\eta^2}+\\&\frac{\alpha^2(n^2-1)^2}{2n^2(n^2+1)}\left[2\frac{\partial\tilde{W}}{\partial\tau}\frac{\partial\tilde{W}}{\partial\eta}\frac{\partial^2\tilde{W}}{\partial\eta\partial\tau}-\tilde{W}\left(\frac{\partial^2\tilde{W}}{\partial\eta\partial\tau}\right)^2+\left(\frac{\partial\tilde{W}}{\partial\tau}\right)^2\frac{\partial^2\tilde{W}}{\partial\eta^2}\right]+\frac{\alpha^4}{2n^2(n^2+1)}\times\\&\left[\frac{\partial^2\tilde{W}}{\partial\eta\partial\tau}\left(\frac{\partial^2\tilde{W}}{\partial\eta\partial\tau}\frac{\partial^2\tilde{W}}{\partial\eta^2}+2\frac{\partial\tilde{W}}{\partial\eta}\frac{\partial^3\tilde{W}}{\partial\eta^2\partial\tau}\right)+\frac{\partial\tilde{W}}{\partial\eta}\left(\frac{\partial\tilde{W}}{\partial\eta}\frac{\partial^4\tilde{W}}{\partial\eta^2\partial\tau^2}+2\frac{\partial^3\tilde{W}}{\partial\eta\partial\tau^2}\frac{\partial^2\tilde{W}}{\partial\eta^2}\right)\right]=0\end{aligned} \tag{20}$$

4.2. Galerkin procedure

Assuming that the solution of nonlinear equation (20) under simply supported boundary conditions is represented as follows (discretization method) [17]

$$\tilde{W}(\eta,\tau)=\tilde{f}_1(\tau)\sin(\pi\eta)+\tilde{f}_2(\tau)\sin(2\pi\eta) \tag{21}$$

we can get the equations of motion for the modal amplitudes $\tilde{f}_1,\tilde{f}_2$ by using the Galerkin method. As the result, we obtain a set of two nonlinear ordinary differential modal equations for $\tilde{f}_1,\tilde{f}_2$ (step ii)

$$\begin{aligned}
&\frac{1}{2}\tilde{f}_2(\tau)\left[4\pi^4\alpha^4+(n^2-1)^4\right]\tilde{f}_1^{'}(\tau)\,\tilde{f}_2^{'}(\tau)+\frac{1}{8}\tilde{f}_1(\tau)\left[3\pi^4\alpha^4+2\pi^2\alpha^2(n^2-1)^2+3(n^2-1)^4\right]\times\\
&\tilde{f}_1^{'}(\tau)^2+\frac{1}{4}\tilde{f}_1(\tau)\left[4\pi^4\alpha^4+5\pi^2\alpha^2(n^2-1)^2+(n^2-1)^4\right]\tilde{f}_2^{'}(\tau)^2+\frac{1}{8}\tilde{f}_1^{''}(\tau)\times\\
&\left\{4\tilde{f}_2(\tau)^2\left[4\pi^4\alpha^4+(n^2-1)^4\right]+\tilde{f}_1(\tau)^2\left[3\pi^4\alpha^4+2\pi^2\alpha^2(n^2-1)^2+3(n^2-1)^4\right]\right\}+\\
&\frac{1}{2}\tilde{f}_1(\tau)\,\tilde{f}_2(\tau)\left[8\pi^4\alpha^4+5\pi^2\alpha^2(n^2-1)^2+2(n^2-1)^4\right]\tilde{f}_2^{''}(\tau)+\frac{1}{2}\pi^4\alpha^4\tilde{f}_1(\tau)^3\times\\
&\left[\pi^2\alpha^2-(n^2-1)^2\right]+2\pi^4\alpha^4\tilde{f}_1(\tau)\,\tilde{f}_2(\tau)^2\left[5\pi^2\alpha^2-2(n^2-1)^2\right]+(\pi^2\alpha^2+n^4+n^2)\,\tilde{f}_1^{''}(\tau)+\\
&\frac{1}{12}\tilde{f}_1(\tau)\left[\pi^4\alpha^4(\beta^2n^4+12)+2\pi^2\alpha^2\beta^2(n^2-1)n^2(\nu+n^2-1)+\beta^2(n^2-1)^2n^4\right]=0
\end{aligned}\tag{22}$$

$$\begin{aligned}
&\frac{1}{2}\tilde{f}_1(\tau)\left[4\pi^4\alpha^4+(n^2-1)^4\right]\tilde{f}_1^{'}(\tau)\,\tilde{f}_2^{'}(\tau)+\frac{1}{4}\tilde{f}_2(\tau)\left[4\pi^4\alpha^4+5\pi^2\alpha^2(n^2-1)^2+(n^2-1)^4\right]\times\\
&\tilde{f}_1^{'}(\tau)^2+\frac{1}{8}\tilde{f}_2(\tau)\left[48\pi^4\alpha^4+8\pi^2\alpha^2(n^2-1)^2+3(n^2-1)^4\right]\tilde{f}_2^{'}(\tau)^2+\frac{1}{4}\tilde{f}_1(\tau)\,\tilde{f}_2(\tau)\times\\
&\left[8\pi^4\alpha^4+5\pi^2\alpha^2(n^2-1)^2+2(n^2-1)^4\right]\tilde{f}_1^{''}(\tau)+\frac{1}{8}\tilde{f}_2^{''}(\tau)\left\{2\tilde{f}_1(\tau)^2\left[4\pi^4\alpha^4+(n^2-1)^4\right]+\right.\\
&\left.\tilde{f}_2(\tau)^2\left[48\pi^4\alpha^4+8\pi^2\alpha^2(n^2-1)^2+3(n^2-1)^4\right]\right\}-8\pi^4\alpha^4\tilde{f}_2(\tau)^3\left[(n^2-1)^2-4\pi^2\alpha^2\right]+\\
&2\pi^4\alpha^4\tilde{f}_1(\tau)^2\,\tilde{f}_2(\tau)\left[5\pi^2\alpha^2-2(n^2-1)^2\right]+(4\pi^2\alpha^2+n^4+n^2)\,\tilde{f}_2^{''}(\tau)+\\
&\frac{1}{12}\tilde{f}_2(\tau)\left[16\pi^4\alpha^4(\beta^2n^4+12)+8\pi^2\alpha^2\beta^2(n^2-1)n^2(\nu+n^2-1)+\beta^2(n^2-1)^2n^4\right]=0
\end{aligned}\tag{23}$$

where $\tilde{f}_i^{'}(\tau)=d\tilde{f}_i(\tau)/d\tau$ and $\tilde{f}_i^{''}(\tau)=d^2\tilde{f}_i(\tau)/d\tau^2$.

This system of nonlinear equations of motion is solved analytically by applying the asymptotic expansion and the multiple scales method, see Ref. [10] for more details.

In this paper, the analytical solution is provided only for the simply supported boundary conditions. The analytical solution also for the clamped-clamped and free-free boundary conditions is reported in detail in Ref. [10].

5. Transition from energy beating to energy localization in SWNTs

In this section, the phenomenon of energy localization in SWNTs is introduced. The dynamical system is conservative (no damping); as an initial condition, a localized energy in one half of the carbon nanotube is given, and it is checked if the energy remains localized forever; different initial excitation amplitudes are considered.

The energy localization is a strongly nonlinear phenomenon, which depends on the amount of the energy provided to the carbon nanotube. Indeed, when the initial energy is quite small, a resonant interaction of two CFMs having close frequencies takes place and the initial localized energy (initial condition) is immediately destroyed, with a periodic redistribution of the energy along the SWNT axis; the time scale of this energy redistribution is inversely proportional to the natural frequencies difference of the CFMs. This process can be interpreted as the beat between two effective particles, each one containing about one half of the SWNT axis: in the case of small amplitude initial energy, a periodic energy exchange between the two halves of the carbon nanotube takes place [6].

When the amplitude of the initial energy is large enough, the nonlinearity preserves the energy localization in the initially excited part of the SWNT [7]. The low-frequency nonlinear oscillations of the SWNTs become localized if the amplitude of the initial energy exceeds a certain threshold, which depends on the SWNT length (for the same chirality). This localization is due to the intensive nonlinear resonant interaction of the two nonlinear normal modes that leads initially to the loss of their stability (intended as single nonlinear normal mode stability). The further development of the resonant interaction (when the energy is increased) leads to the confinement of the vibration energy in one half only of the nanotube. In this case, the beating phenomenon and the energy exchange are generally locked and the total energy is trapped in the initial excitation domain. The amplitude of the smallest initial excitation, corresponding to the energy confinement in one half of the SWNT axis, is called “energy localization threshold” [10].

In this section, the transition from energy beating to energy localization is investigated by using numerical and analytical approaches; the results are then compared with Molecular Dynamics (MD) simulations, for validation.

5.1. Numerical method

Considering the lagrangian coordinates $\tilde{f}_j(\tau)$ of the expansions (11) and assuming the modal initial conditions $\tilde{f}_1(0) = \tilde{f}_2(0) = \tilde{f}(0)$, the amplitude of the initial excitation $\tilde{X}(0)$ can be written as [10]

$$\tilde{X}(0) = \frac{\tilde{f}^2(0)}{2\varepsilon^2}(\tilde{\omega}_1 + \tilde{\omega}_2) \tag{24}$$

where the natural small parameter ε denotes the relative difference between the nondimensional natural frequencies of the two lowest CFMs $(\tilde{\omega}_1, \tilde{\omega}_2)$ [10]

$$\varepsilon = \sqrt{\frac{\tilde{\omega}_2 - \tilde{\omega}_1}{\tilde{\omega}_1}} \tag{25}$$

It should be highlighted that in the present paper the initial velocities are taken equal to zero (the modal initial conditions are imposed only on the displacements).

Once obtained the value of the modal initial conditions on the displacements to which corresponds the energy localization on the carbon nanotube axis $\tilde{f}(0)_{\text{loc}}$, by substituting this value in equation (24) it is possible to achieve the value of the localization threshold $\tilde{X}(0)_{\text{loc}}$ as

$$\tilde{X}(0)_{\text{loc}} = \frac{\tilde{f}_{\text{loc}}^2(0)}{2\varepsilon^2}(\tilde{\omega}_1 + \tilde{\omega}_2) \tag{26}$$

where the localization threshold $\tilde{X}(0)_{\text{loc}}$ represents the amplitude of the initial external excitation $\tilde{X}(0)$ which involves the complete energy localization in one half of the SWNT.

In Figure 2, the time evolution of the total energy distribution along the axis of a simply supported SWNT is reported, the aspect ratio is $L/R = 20$, the numerical method and equation (24) are used for obtaining results: for such carbon nanotube, the numerical value of the energy localization threshold is equal to $\tilde{X}(0)_{\text{loc}} = 0.14593$.

In Figure 2(a), the amplitude of initial excitation is $\tilde{X}(0) = 0.080$ (lower than the energy threshold), and a periodic energy exchange between the two halves of the SWNT axis takes place. It should be noted that the initial excitation domain ($\tau = 0$) corresponds to the second half of the nanotube axis

$(0.5 \leq \eta \leq 1)$ (localized initial energy); the time evolution shows that the localization is promptly lost and the energy spreads on the first half as well.

In Figure 2(b), the amplitude of initial excitation is $\tilde{X}(0) = 0.160$ (higher than the energy threshold), and an energy localization in the second half of the SWNT axis (initial excitation domain) is given; in this case, the time evolution shows that the energy never flows toward the first half of the carbon nanotube, and a perfect confinement of energy is manifested.

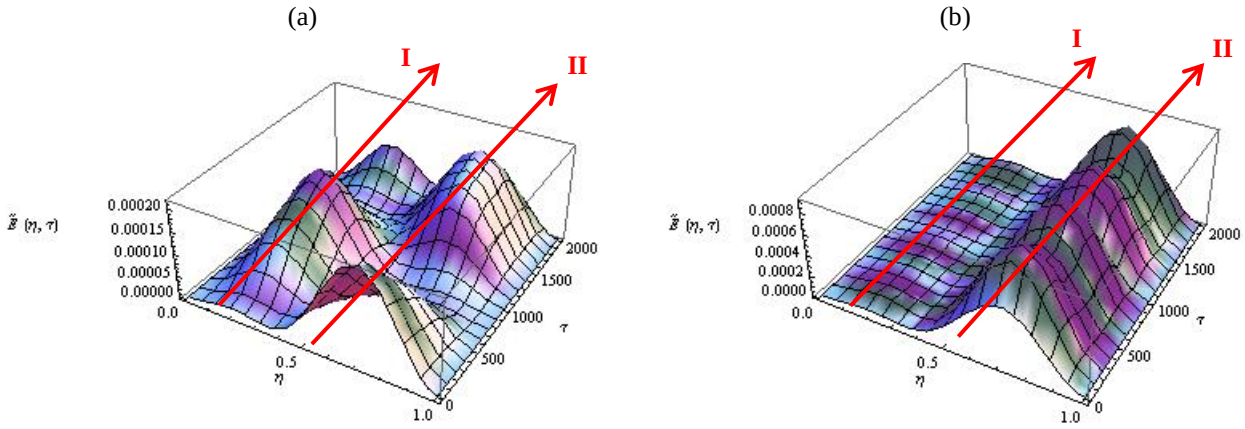

Figure 2. Time evolution of the total energy distribution along the axis of a simply supported SWNT; L/R = 20; numerical method; equivalent parameters of Table 1; energy localization threshold $\tilde{X}(0)_{\text{loc}} = 0.14593$. (a) Initial excitation amplitude $\tilde{X}(0) = 0.080$ (no localization). (b) Initial excitation amplitude $\tilde{X}(0) = 0.160$ (energy localization).

5.2. Analytical method

Applying the asymptotic expansion and multiple scales analytical method to the general solutions (22-23), the following two equations of motion can be obtained [10]

$$\begin{aligned} i\frac{\partial \tilde{\chi}_1}{\partial \tau} + \tilde{a}_1 \left|\tilde{\chi}_1\right|^2 \tilde{\chi}_1 + \tilde{a}_3 \left|\tilde{\chi}_2\right|^2 \tilde{\chi}_1 + \tilde{a}_4 \tilde{\chi}_2^2 \tilde{\chi}_1^* = 0 \\ i\frac{\partial \tilde{\chi}_2}{\partial \tau} + \tilde{\omega}_1 \tilde{\chi}_2 + \tilde{a}_3 \left|\tilde{\chi}_2\right|^2 \tilde{\chi}_1 + \tilde{a}_2 \left|\tilde{\chi}_2\right|^2 \tilde{\chi}_2 + \tilde{a}_4 \tilde{\chi}_1^2 \tilde{\chi}_2^* = 0 \end{aligned} \tag{27}$$

where ($\tilde{\chi}_1, \tilde{\chi}_2$) denote the nondimensional complex amplitudes of the two nonlinear normal CFMs, ($\tilde{\chi}_1^*, \tilde{\chi}_2^*$) are the correspondent complex conjugate amplitudes, $\tilde{a}_j$ are nondimensional coefficients depending on SWNT mechanical parameters and $\tilde{\omega}_1$ is the lower nondimensional natural frequency. The energy integral of equations (27) corresponds to the nondimensional Hamiltonian function [10]

$$\tilde{H} = \tilde{\omega}_1 \left|\tilde{\chi}_2\right|^2 + \tilde{a}_1 \left|\tilde{\chi}_1\right|^4 + \tilde{a}_2 \left|\tilde{\chi}_2\right|^4 + \tilde{a}_3 \left|\tilde{\chi}_1\right|^2 \left|\tilde{\chi}_2\right|^2 + \tilde{a}_4 \left(\tilde{\chi}_1^2 \tilde{\chi}_2^{*2} + \tilde{\chi}_1^{*2} \tilde{\chi}_2^2\right) \tag{28}$$

The nondimensional complex amplitudes ($\tilde{\chi}_1, \tilde{\chi}_2$) define the occupation number integral as [9]

$$\tilde{X}(0) = \left|\tilde{\chi}_1\right|^2 + \left|\tilde{\chi}_2\right|^2 \tag{29}$$

which describes the initial excitation level, similarly to equation (24) of the numerical approach, representing a first integral of equation (27).

The linear combination of the nonlinear normal CFMs $(\tilde{\chi}_1, \tilde{\chi}_2)$ defines two new variables $(\tilde{\psi}_1, \tilde{\psi}_2)$, called “effective particles”, which are written in the following form [9]

$$\tilde{\psi}_1 = \frac{1}{\sqrt{2}}\left(\tilde{\chi}_1 + \tilde{\chi}_2\right) \qquad \tilde{\psi}_2 = \frac{1}{\sqrt{2}}\left(\tilde{\chi}_1 - \tilde{\chi}_2\right) \tag{30}$$

and are related to the occupation number integral $\tilde{X}(0)$ in the form [9]

$$\tilde{X}(0) = \left|\tilde{\psi}_1\right|^2 + \left|\tilde{\psi}_2\right|^2 \tag{31}$$

In particular, the effective particles $(\tilde{\psi}_1, \tilde{\psi}_2)$ describe the nonlinear dynamics and energy exchange of the two halves of the SWNT similarly to some groups of particles in the discrete one-dimensional oscillatory chain [6].

Really, by considering the energy distribution along the SWNT axis, one can see that such a linear combination of normal CFMs describes an energy concentration in a certain region of the SWNT, while the other part of the SWNT has a lower energy density; therefore, these regions can be seen as elementary blocks, identified as "effective particles", which demonstrate behaviour similar to a system of two weakly coupled oscillators [6].

The occupation number integral $\tilde{X}(0)$ (29) allows the phase space of the SWNT to be reduced up to the 2 dimensions (Θ, Δ), where the first variable Θ defines the relative amplitude of the effective particles and the second one Δ corresponds to the phase shift between them; therefore, the effective particles $(\tilde{\psi}_1, \tilde{\psi}_2)$ can be expressed in terms of the amplitude Θ and phase shift Δ as follows [10]

$$\tilde{\psi}_1 = \sqrt{\tilde{X}(0)}\cos(\Theta)e^{-i\Delta/2} \qquad \tilde{\psi}_2 = \sqrt{\tilde{X}(0)}\sin(\Theta)e^{i\Delta/2} \tag{32}$$

Substituting the equations (29), (30), (32) into the equation (28), the nondimensional Hamiltonian function $\tilde{H}$ takes the following expression in terms of the angular variables Θ and Δ [10]

$$\tilde{H}(\Theta,\Delta) = \frac{\tilde{X}(0)}{16}\Big\{8\tilde{a}_0\left(1-\cos(\Delta)\sin(2\Theta)\right) + \tilde{X}(0)\Big[2\tilde{a}_4\left(2\cos^2(\Delta) - \left(\cos(2\Delta)-3\right)\cos(4\Theta)\right) + \tilde{a}_3\left(2\cos^2(\Delta)\cos(4\Theta) - \cos(2\Delta) + 3\right) + 4\tilde{a}_2\left(\cos(\Delta)\sin(2\Theta) - 1\right)^2 + 4\tilde{a}_1\left(\cos(\Delta)\sin(2\Theta) + 1\right)^2\Big]\Big\} \tag{33}$$

In Figure 3, two phase portraits describing the total energy vs. the Hamiltonian variables (Θ, Δ) are shown, the same SWNT of Figure 2 is considered, results are obtained by considering the analytical method and Hamiltonian function (33): for such carbon nanotube, the analytical value of the energy localization threshold is equal to $\tilde{X}(0)_{\text{loc}} = 0.14283$.

In Figure 3(a), the same initial excitation amplitude $\tilde{X}(0) = 0.080$ of Figure 2(a) is applied (lower than energy threshold); two steady states ($\Delta = 0$, $\Theta = \pi/4$) and ($\Delta = \pi$, $\Theta = \pi/4$) are present, which correspond to the nonlinear normal CFMs $(\tilde{\chi}_1, \tilde{\chi}_2)$, respectively (stationary points); the values ($\Theta = 0$) and ($\Theta = \pi/2$) describe the energy concentration on the effective particles $(\tilde{\psi}_1, \tilde{\psi}_2)$, respectively.

The phase trajectories surrounding the stationary points $(\tilde{\chi}_1, \tilde{\chi}_2)$ describe the nonlinear dynamics of the SWNT; the phase trajectories maximally distant from the stationary points are called "Limiting Phase Trajectories" (LPTs).

In this phase portrait, the motion along the LPTs describes the energy exchange between the two effective particles $(\tilde{\psi}_1, \tilde{\psi}_2)$, which corresponds to the energy beating between the two halves of the SWNT axis.

In particular, the lower effective particle $\tilde{\psi}_1(\Theta = 0)$ corresponds to the first half ($0 \le \eta \le 0.5$) of the SWNT axis; the upper effective particle $\tilde{\psi}_2(\Theta = \pi/2)$ corresponds to the second half ($0.5 \le \eta \le 1$) of the SWNT axis.

By supposing that the initial excitation domain (τ = 0) corresponds to the upper effective particle $\tilde{\psi}_2$ (localized initial energy), from Figure 3(a) it can be seen that, in the case of small amplitude initial energy, a periodic energy exchange between the two effective particles (each one contains about one half of the SWNT axis) takes place; in this specific dynamic state, the energy distribution along the SWNT axis is the most non-uniform one (energy beating phenomenon between the two parts of the SWNT).

In Figure 3(b), the same initial excitation amplitude $\tilde{X}(0) = 0.160$ of Figure 2(b) is applied (higher than energy threshold); the steady state ($\Delta = \pi$, $\Theta = \pi/4$) is present, which corresponds to the higher frequency nonlinear normal CFM $\tilde{\chi}_2$ (second initial stationary point); two additional steady states ($\Delta = 0$, $\Theta = 3\pi/16$) and ($\Delta = 0$, $\Theta = 5\pi/16$) arise, as the result of the instability of the lower frequency nonlinear normal CFM $\tilde{\chi}_1$ (first initial stationary point), which are called $\tilde{\chi}_1^{'}$ and $\tilde{\chi}_1^{''}$, respectively; the two effective particles $\tilde{\psi}_1(\Theta = 0)$ and $\tilde{\psi}_2(\Theta = \pi/2)$ are still present.

By supposing that the initial excitation domain (τ = 0) corresponds to the upper effective particle $\tilde{\psi}_2$ (localized initial energy), from Figure 3(b) it can be seen that in the case of high amplitude initial energy, a complete energy localization in the upper effective particle (initial excitation domain) is present, which corresponds to the second half of the nanotube axis: any limiting phase trajectory, starting from the upper effective particle $\tilde{\psi}_2$ (initial excitation), cannot reach the lower one $\tilde{\psi}_1$.

In this specific dynamic state, the energy distribution along the SWNT axis is the most uniform one (energy localization phenomenon in the initial excited part of the SWNT): the beating phenomenon and energy exchange are locked, where the total energy is trapped in the initial excitation domain.

It is to be reminded that the amplitude of the smallest initial excitation, corresponding to the energy confinement in one half of the SWNT axis, is called "energy localization threshold" [10].

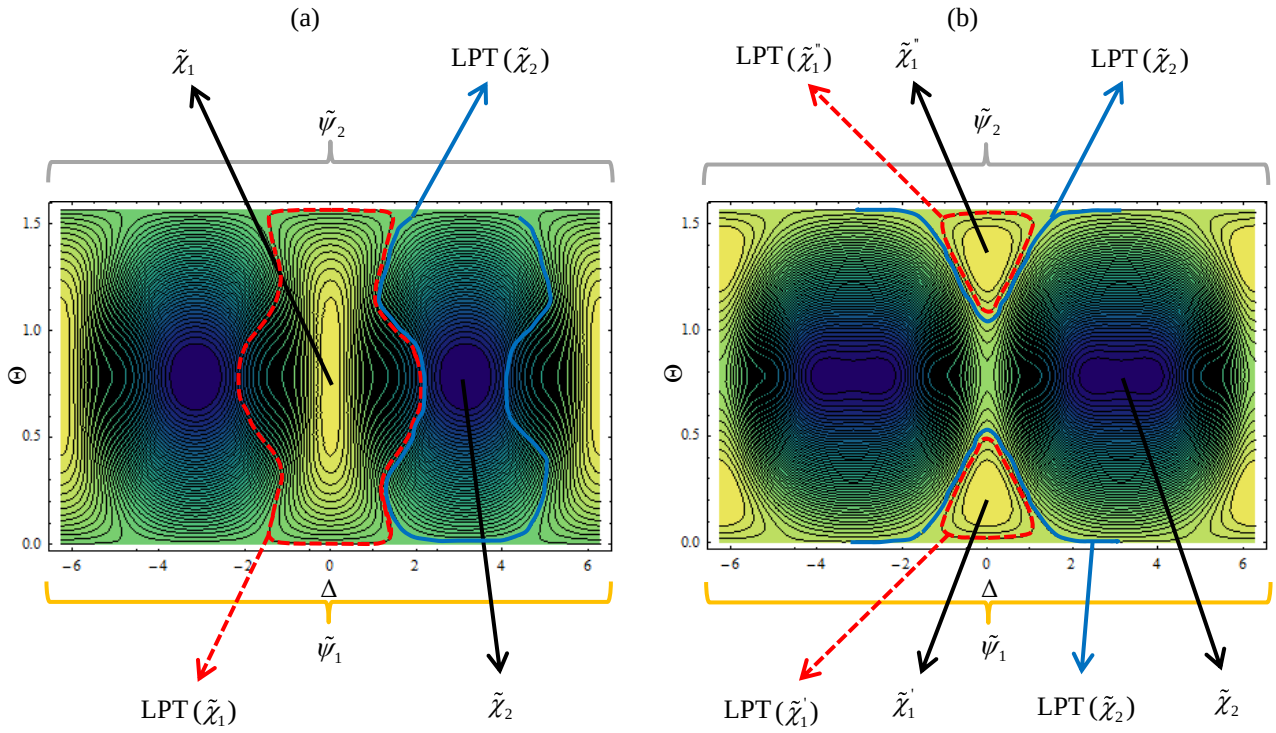

Figure 3. Total energy vs. the Hamiltonian variables (Θ, Δ); simply supported SWNT; L/R = 20; analytical method; equivalent parameters of Table 1; energy localization threshold $\tilde{X}(0)_{\text{loc}} = 0.14283$. (a) Initial excitation amplitude $\tilde{X}(0) = 0.080$ (no localization). (b) Initial excitation amplitude $\tilde{X}(0) = 0.160$ (energy localization).

5.3. Molecular Dynamics (MD) simulations

In order to verify the results of the numerical and analytical approaches on the nonlinear transition from energy beating to energy localization in SWNTs, Molecular Dynamics (MD) simulations were performed; realistic inter-atomic potential functions were considered for the calculation of the total potential energy of the system; force fields containing the energies of the covalent C-C bonding, valence and torsion angle deformation, Van-der-Waals interaction were applied.

The MD simulations were divided into subsequent stages. At the first stage, the SWNT was kept at approximately 400K in order to obtain a high-temperature structural relaxation. At the second stage, the temperature of the SWNT was decreased with a constant rate down to approximately 1K with a subsequent low-temperature structural relaxation. The third stage dealt with the SWNT deformation according to the analytical solution (21) with subsequent structural relaxation (initial conditions on the displacements); the second version of the initial conditions consisted in the determination of the initial velocities of atoms at zero initial displacements. After these stages, the external fields were turned off allowing free SWNT oscillations. In accordance with the analytical description (21), the atoms at the SWNT edges were fixed against radial displacements in order to respect the imposed simply supported boundary conditions.

In Figure 4, the time evolution of the total energy distribution along the axis of a simply supported SWNT is shown, the nanotube is the same of Figure 2, different values of the oscillation amplitude (initial excitation) are considered; the SWNT is divided into 60 elementary rings ($1 \leq Z \leq 60$), each of them containing 40 carbon atoms.

When the initial excitation is lower that the value of localization threshold, Figure 4(a), a periodic energy exchange between the two halves of the SWNT axis takes place (energy beating).

When the initial excitation is higher that the value of localization threshold, Figure 4(b), an energy localization takes place in one half of the SWNT axis (initial excitation domain).

Therefore, the MD simulations confirm the results of the numerical and analytical approaches in the nonlinear field, see Ref. [10] for more details on the MD simulations techniques and inter-atomic potential functions.

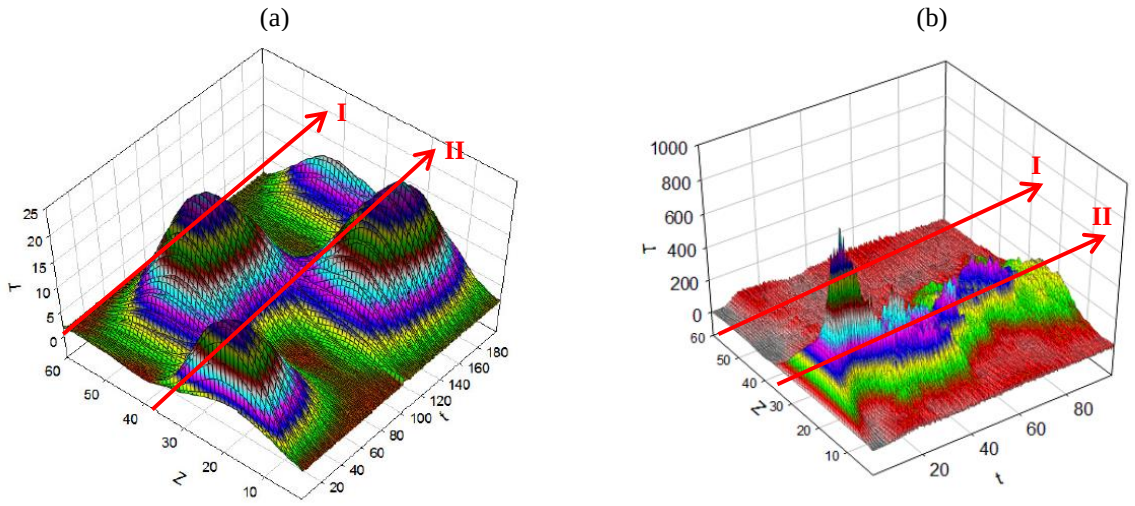

Figure 4. Time evolution of the total energy distribution along the axis of a simply supported SWNT; L/R = 20; MD simulations; equivalent parameters of Table 1; energy localization threshold $\tilde{X}(0)_{\text{loc}} = 0.14593$. (a) Initial excitation amplitude $\tilde{X}(0) = 0.130$ (no localization). (b) Initial excitation amplitude $\tilde{X}(0) = 0.160$ (energy localization).

6. Numerical results

The mechanical parameters of the SWNT analysed in this paper are shown in Table 1.

In Table 2, comparisons between natural frequencies obtained using the Sanders-Koiter continuum thin shell theory and MD simulations [11] are reported.

A nonlinear convergence analysis is carried out for the numerical method in order to select the correct number of axisymmetric and asymmetric modes; different nonlinear modal expansions and boundary conditions are analysed.

The analytical and numerical values of the nonlinear energy localization threshold are estimated for different aspect ratios of the SWNT; the influence of the boundary conditions is investigated.

Young's modulus E [TPa]	5.5
Poisson's ratio ν	0.19
Mass density ρ [kg/m^3]	11700
Thickness h [nm]	0.066
Radius R [nm]	0.786

Table 1. Mechanical parameters of the SWNT [17].

Natural frequency (THz)			Difference %
L = 5.614 nm	SKT – Present model	MDS – Ref. [11]	
first mode	0.0827	0.0793	4.34
second mode	0.4741	0.4486	5.68
third mode	1.1854	1.1139	6.42
fourth mode	2.0565	1.9134	7.48
fifth mode	3.0082	2.7802	8.20
L = 14.16 nm	SKT – Present model	MDS – Ref. [11]	
first mode	0.0142	0.0138	3.25
second mode	0.0828	0.0794	4.26
third mode	0.2241	0.2138	4.81
fourth mode	0.4297	0.4069	5.61
fifth mode	0.6808	0.6414	6.15
L = 23.96 nm	SKT – Present model	MDS – Ref. [11]	
first mode	0.0047	0.0046	2.17
second mode	0.0290	0.0282	2.84
third mode	0.0803	0.0778	3.21
fourth mode	0.1551	0.1495	3.74
fifth mode	0.2541	0.2441	4.10

Table 2. Natural frequencies of the clamped-free SWNT with radius R = 0.339 nm and different lengths L. Comparisons between Sanders-Koiter shell theory (SKT) and Molecular Dynamics Simulations (MDS).

In Table 2, comparisons between the natural frequencies of a clamped-free SWNT with radius R = 0.339 nm and different lengths L obtained by using the Sanders-Koiter continuum thin shell theory and MD simulations are reported; these comparisons allow the classical continuum thin shell theory applied in the present work to be validated in the linear field by means of MD simulations results retrieved from the pertinent literature [11].

6.1. Nonlinear convergence analysis

The first step of the nonlinear analysis for the numerical approach is the convergence check in terms of the modal expansions (11); it is carried out on SWNTs with L/R = 20 and different boundary conditions, in order to select the correct number and type of vibration modes providing an accurate result in nonlinear field.

An initial two-mode approximation involves: i) the resonant modes (1,2) and (2,2) for the simply supported and clamped boundary conditions; ii) the resonant modes (0,2) and (1,2) for the free-free boundary conditions. The convergence is then checked by adding suitable modes to the resonant ones, i.e., asymmetric modes with higher wave numbers (quadratic and cubic nonlinearities) and axisymmetric modes (quadratic nonlinearities).

The convergence is reached with a 24 dof model (Tables 3-8), described in the following, which is assumed as reference model; the percentage root mean square time domain error ($\mathrm{ERROR_{RMS}}$%) is adopted as convergence parameter, which is expressed by the following formula:

$$\mathrm{ERROR_{RMS}}\% = \sqrt{\frac{1}{\tilde{T}}\int_0^{\tilde{T}}\left[\frac{\tilde{q}_n(\tau)-\tilde{q}_{24}(\tau)}{\max(\tilde{q}_{24}(\tau))}\right]^2 d\tau}\times 100 \tag{34}$$

where: $\tilde{q}_n(\tau)$ denotes the sum of the radial time histories of the resonant modes; $\max(\tilde{q}_{24}(\tau))$ is the maximum value of parameter $\tilde{q}_{24}(\tau)$; $\tilde{T}$ is a suitably long nondimensional time ($\tilde{T} = 2000$).

In Figures 5-6 and Tables 3-4, the convergence analysis for the numerical method in the case of simply supported boundary conditions is reported. Time histories and energy distributions obtained by considering nonlinear modal expansions with different degrees of freedom are compared for the aspect ratio L/R = 20. The corresponding energy localization threshold is $\tilde{X}(0)_{\mathrm{loc}} = 0.14593$ and the modal expansion with 24 dof is assumed as the reference ($\mathrm{ERROR_{RMS}}$% = 0).

In Figure 5 and Table 3 the initial excitation amplitude $\tilde{X}(0) = 0.140$ is considered (lower than the threshold, $\tilde{X}(0) < \tilde{X}(0)_{\mathrm{loc}}$). All the considered models converge to a nonlinear behaviour which is very similar to the 24 dof modal expansion with a right energy beating.

In Figure 6 and Table 4 the initial excitation amplitude $\tilde{X}(0) = 0.150$ is considered (higher than the threshold, $\tilde{X}(0) > \tilde{X}(0)_{\mathrm{loc}}$). The 8 dof model shows a nonlinear behaviour very different from the 24 dof one, with a wrong energy beating; conversely, models from 14 to 22 dof converge to a nonlinear behaviour very similar to the 24 dof modal expansion, with an energy localization.

From the previous analyses, it can be observed that 16-22-24 dof expansions behave quite similarly and the smallest expansion able to predict the dynamics with acceptable accuracy is the 16 dof model ($ERROR_{RMS}\% = 5 \div 6$). The main weakness of 8 dof model is the insufficient number of asymmetric and axisymmetric modes, which are very important for properly modelling the bending deformation – asymmetric modes (1,4),(2,4) – and the circumferential stretching – axisymmetric mode (2,0) – during the modal vibration. A similar behaviour has been obtained for the convergence analysis of nonlinear amplitude-frequency curves of FGM circular cylindrical shells, see Ref. [38], where it was confirmed that, in nonlinear field, the axisymmetric modes play a role of primary importance.

(*j*,*n*)	(1,2)	(2,2)	(3,2)	(1,4)	(2,4)	(3,4)	(1,0)	(2,0)	(3,0)	$ERROR_{RMS}\%$
8 dof model	*u*, *v*, *w*	*u*, *v*, *w*	–	–	–	–	*u*, *w*	–	–	14.01
14 dof model	*u*, *v*, *w*	*u*, *v*, *w*	–	*u*, *v*, *w*	*u*, *v*, *w*	–	*u*, *w*	–	–	8.93
16 dof model	***u*, *v*, *w***	***u*, *v*, *w***	**–**	***u*, *v*, *w***	***u*, *v*, *w***	**–**	***u*, *w***	***u*, *w***	**–**	**4.70**
22 dof model	*u*, *v*, *w*	*u*, *v*, *w*	*u*, *v*, *w*	*u*, *v*, *w*	*u*, *v*, *w*	*u*, *v*, *w*	*u*, *w*	*u*, *w*	–	1.89
24 dof model	*u*, *v*, *w*	*u*, *v*, *w*	*u*, *v*, *w*	*u*, *v*, *w*	*u*, *v*, *w*	*u*, *v*, *w*	*u*, *w*	*u*, *w*	*u*, *w*	

Table 3. Convergence analysis. Numerical method. Nonlinear modal expansions (11). $ERROR_{RMS}\%$ in time domain. 24 dof model reference. Simply supported boundary conditions. Aspect ratio $L/R = 20$. Initial amplitude $\tilde{X}(0) < \tilde{X}(0)_{loc}$.

(*j*,*n*)	(1,2)	(2,2)	(3,2)	(1,4)	(2,4)	(3,4)	(1,0)	(2,0)	(3,0)	$ERROR_{RMS}\%$
8 dof model	*u*, *v*, *w*	*u*, *v*, *w*	–	–	–	–	*u*, *w*	–	–	82.22
14 dof model	*u*, *v*, *w*	*u*, *v*, *w*	–	*u*, *v*, *w*	*u*, *v*, *w*	–	*u*, *w*	–	–	12.75
16 dof model	***u*, *v*, *w***	***u*, *v*, *w***	**–**	***u*, *v*, *w***	***u*, *v*, *w***	**–**	***u*, *w***	***u*, *w***	**–**	**5.68**
22 dof model	*u*, *v*, *w*	*u*, *v*, *w*	*u*, *v*, *w*	*u*, *v*, *w*	*u*, *v*, *w*	*u*, *v*, *w*	*u*, *w*	*u*, *w*	–	2.51
24 dof model	*u*, *v*, *w*	*u*, *v*, *w*	*u*, *v*, *w*	*u*, *v*, *w*	*u*, *v*, *w*	*u*, *v*, *w*	*u*, *w*	*u*, *w*	*u*, *w*	

Table 4. Convergence analysis. Numerical method. Nonlinear modal expansions (11). $ERROR_{RMS}\%$ in time domain. 24 dof model reference. Simply supported boundary conditions. Aspect ratio $L/R = 20$. Initial amplitude $\tilde{X}(0) > \tilde{X}(0)_{loc}$.

Case	Time history	Energy distribution
8 dof model	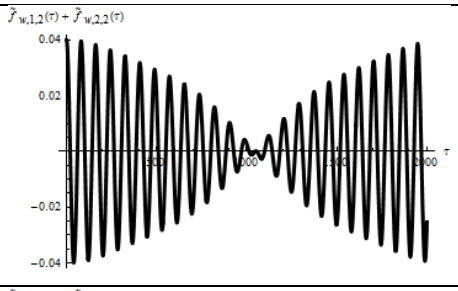	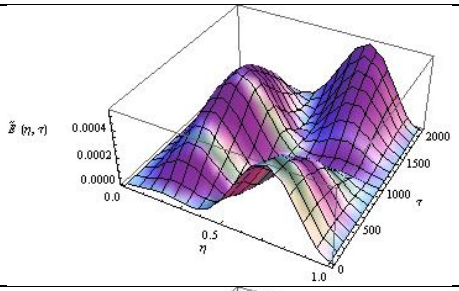
14 dof model	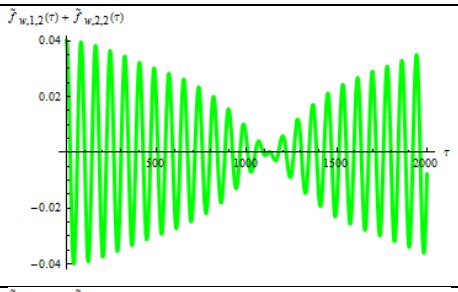	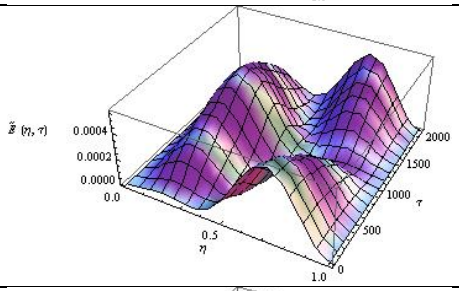
16 dof model	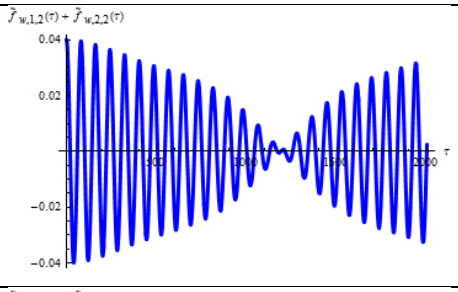	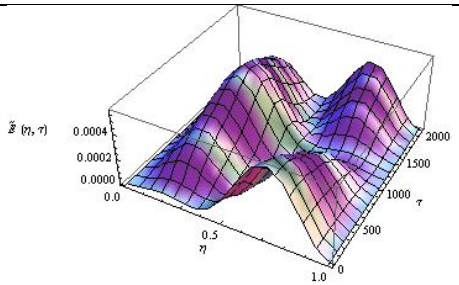
22 dof model	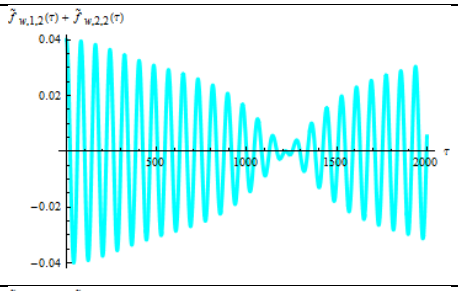	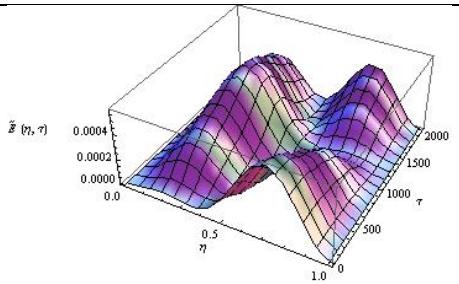
24 dof model	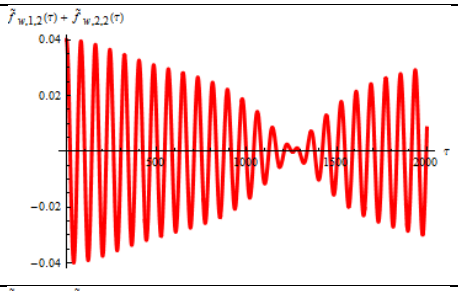	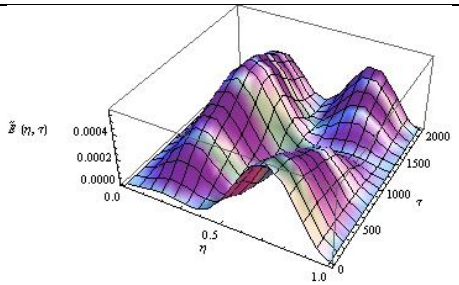
comparisons	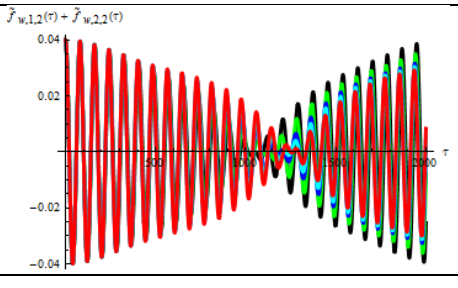	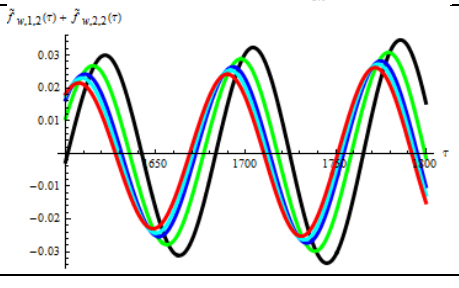

Figure 5. Convergence analysis. Numerical method. Nonlinear modal expansions (11). Simply supported boundary conditions. Aspect ratio $L/R = 20$. $\tilde{X}(0) < \tilde{X}(0)_{\text{loc}}$ "—", 8 dof. "—", 14 dof. "—", 16 dof. "—", 22 dof. "—", 24 dof.

Case	Time history	Energy distribution
8 dof model	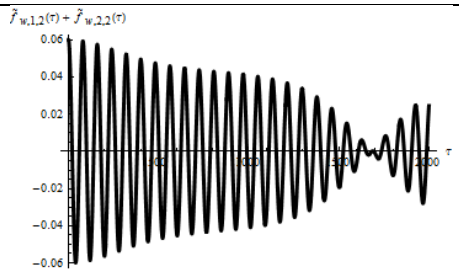	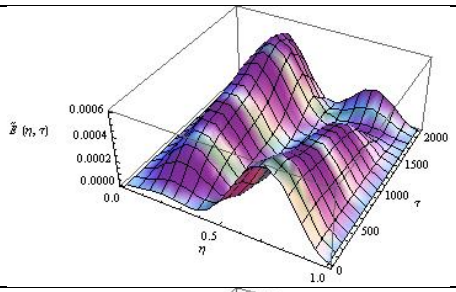
14 dof model	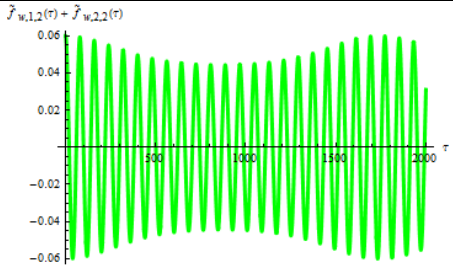	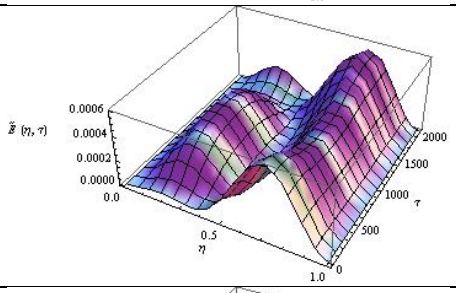
16 dof model	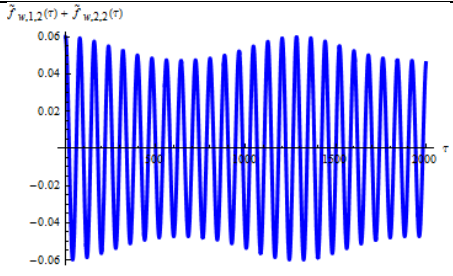	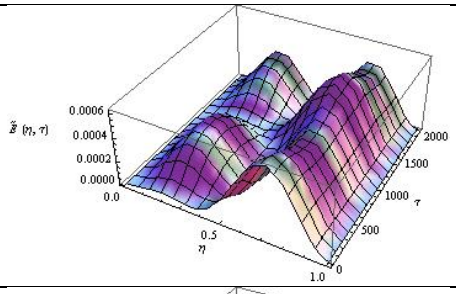
22 dof model	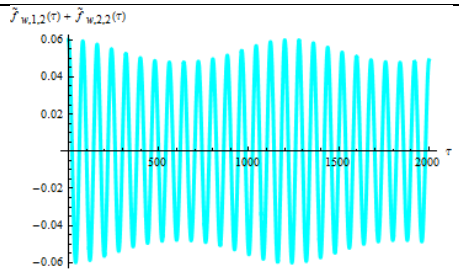	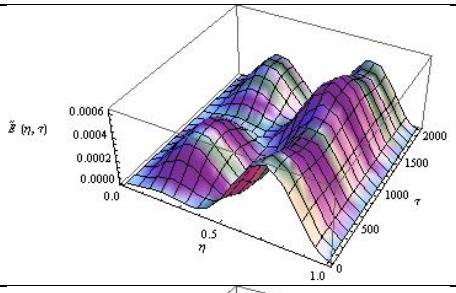
24 dof model	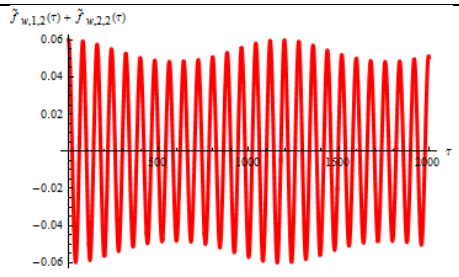	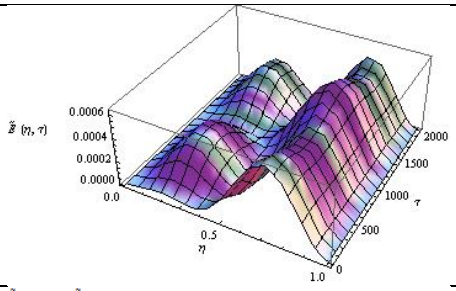
comparisons	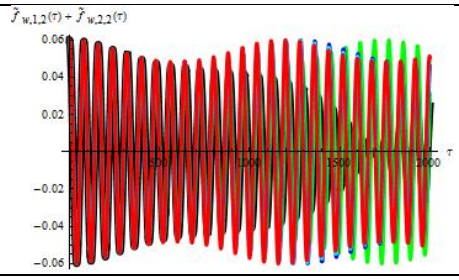	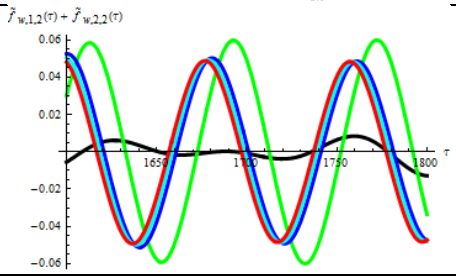

Figure 6. Convergence analysis. Numerical method. Nonlinear modal expansions (11). Simply supported boundary conditions. Aspect ratio $L/R = 20$. $\tilde{X}(0) > \tilde{X}(0)_{\text{loc}}$ "—", 8 dof. "—", 14 dof. "—", 16 dof. "—", 22 dof. "—", 24 dof.

In Figures 7-8 and Tables 5-6, the convergence analysis for the numerical method in the case of clamped-clamped boundary conditions is reported. Time histories and energy distributions obtained by considering different expansions are compared for the aspect ratio L/R = 20. The corresponding energy localization threshold is $\tilde{X}(0)_{\text{loc}} = 0.17020$ and the modal expansion with 24 dof is assumed as the reference ($\text{ERROR}_{\text{RMS}}\% = 0$).

In Figure 7 and Table 5 the initial excitation amplitude $\tilde{X}(0) = 0.160$ is considered (lower than the threshold, $\tilde{X}(0) < \tilde{X}(0)_{\text{loc}}$). All models converge to a nonlinear behaviour very similar to the 24 dof model, with an energy beating.

In Figure 8 and Table 6 the initial excitation amplitude $\tilde{X}(0) = 0.180$ is considered (higher than the threshold, $\tilde{X}(0) > \tilde{X}(0)_{\text{loc}}$). The 8 dof model shows a nonlinear behaviour very different from the 24 dof one, with a wrong energy beating; conversely, the higher-order models from 14 to 22 dof converge to a nonlinear behaviour very similar to the 24 dof model, with an energy localization.

Similarly to the case of simply supported boundary conditions, from the previous analyses it can be observed that, also in the case of clamped edges, the 16-22-24 dof expansions behave quite similarly and the smallest expansion able to predict the dynamics with acceptable accuracy is the 16 dof model ($\text{ERROR}_{\text{RMS}}\% = 5 \div 6$).

(j,n)	(1,2)	(2,2)	(3,2)	(1,4)	(2,4)	(3,4)	(1,0)	(2,0)	(3,0)	$\text{ERROR}_{\text{RMS}}$%
8 dof model	*u*, *v*, *w*	*u*, *v*, *w*	–	–	–	–	*u*, *w*	–	–	15.64
14 dof model	*u*, *v*, *w*	*u*, *v*, *w*	–	*u*, *v*, *w*	*u*, *v*, *w*	–	*u*, *w*	–	–	9.41
16 dof model	***u*, *v*, *w***	***u*, *v*, *w***	**–**	***u*, *v*, *w***	***u*, *v*, *w***	**–**	***u*, *w***	***u*, *w***	**–**	**4.82**
22 dof model	*u*, *v*, *w*	*u*, *v*, *w*	*u*, *v*, *w*	*u*, *v*, *w*	*u*, *v*, *w*	*u*, *v*, *w*	*u*, *w*	*u*, *w*	–	2.01
24 dof model	*u*, *v*, *w*	*u*, *v*, *w*	*u*, *v*, *w*	*u*, *v*, *w*	*u*, *v*, *w*	*u*, *v*, *w*	*u*, *w*	*u*, *w*	*u*, *w*	

Table 5. Convergence analysis. Numerical method. Nonlinear modal expansions (11). $\text{ERROR}_{\text{RMS}}$% in time domain. 24 dof model reference. Clamped-clamped boundary conditions. Aspect ratio $L/R = 20$. Initial amplitude $\tilde{X}(0) < \tilde{X}(0)_{\text{loc}}$.

(j,n)	(1,2)	(2,2)	(3,2)	(1,4)	(2,4)	(3,4)	(1,0)	(2,0)	(3,0)	$\text{ERROR}_{\text{RMS}}$%
8 dof model	*u*, *v*, *w*	*u*, *v*, *w*	–	–	–	–	*u*, *w*	–	–	85.48
14 dof model	*u*, *v*, *w*	*u*, *v*, *w*	–	*u*, *v*, *w*	*u*, *v*, *w*	–	*u*, *w*	–	–	13.71
16 dof model	***u*, *v*, *w***	***u*, *v*, *w***	**–**	***u*, *v*, *w***	***u*, *v*, *w***	**–**	***u*, *w***	***u*, *w***	**–**	**5.92**
22 dof model	*u*, *v*, *w*	*u*, *v*, *w*	*u*, *v*, *w*	*u*, *v*, *w*	*u*, *v*, *w*	*u*, *v*, *w*	*u*, *w*	*u*, *w*	–	2.76
24 dof model	*u*, *v*, *w*	*u*, *v*, *w*	*u*, *v*, *w*	*u*, *v*, *w*	*u*, *v*, *w*	*u*, *v*, *w*	*u*, *w*	*u*, *w*	*u*, *w*	

Table 6. Convergence analysis. Numerical method. Nonlinear modal expansions (11). $\text{ERROR}_{\text{RMS}}$% in time domain. 24 dof model reference. Clamped-clamped boundary conditions. Aspect ratio $L/R = 20$. Initial amplitude $\tilde{X}(0) > \tilde{X}(0)_{\text{loc}}$.

Case	Time history	Energy distribution
8 dof model	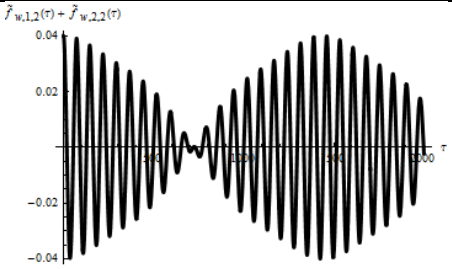	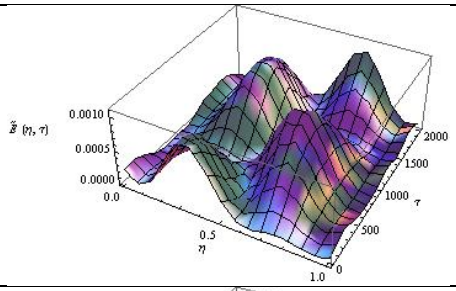
14 dof model	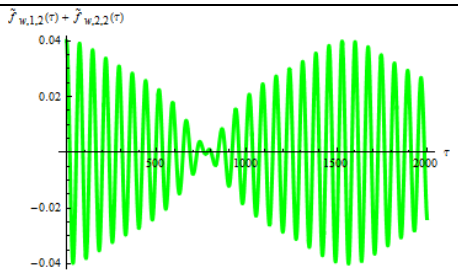	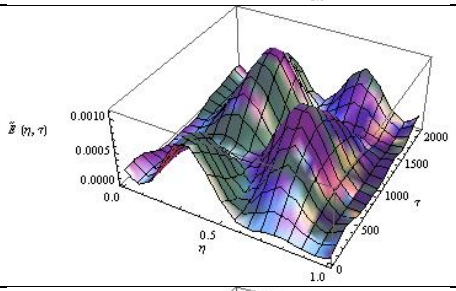
16 dof model	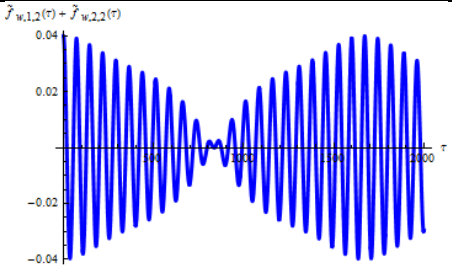	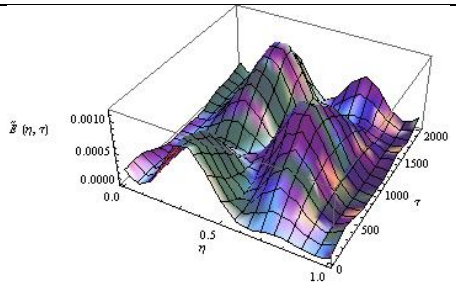
22 dof model	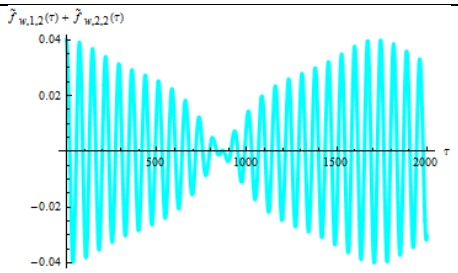	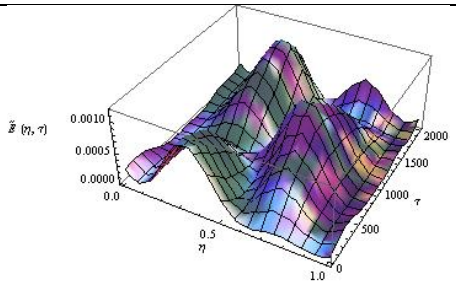
24 dof model	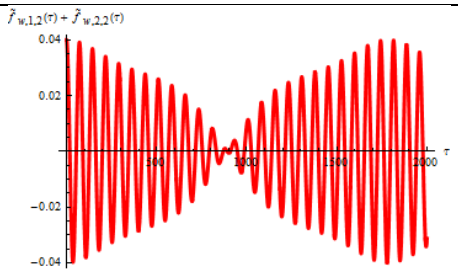	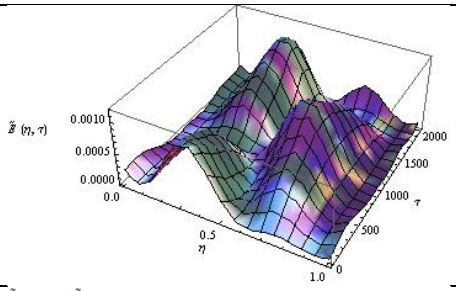
comparisons	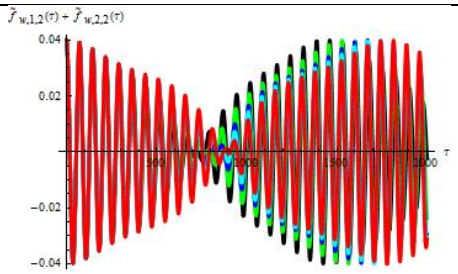	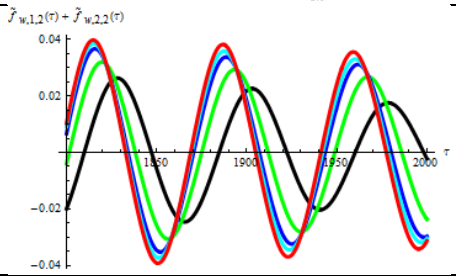

Figure 7. Convergence analysis. Numerical method. Nonlinear modal expansions (11). Clamped-clamped boundary conditions. Aspect ratio $L/R = 20$. $\tilde{X}(0) < \tilde{X}(0)_{\text{loc}}$ "—", 8 dof. "—", 14 dof. "—", 16 dof. "—", 22 dof. "—", 24 dof.

Case	Time history	Energy distribution
8 dof model	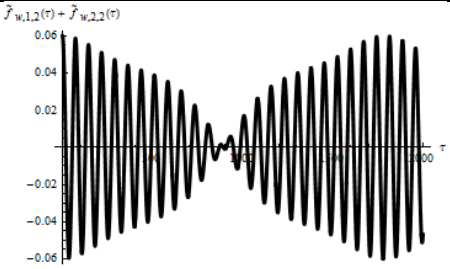	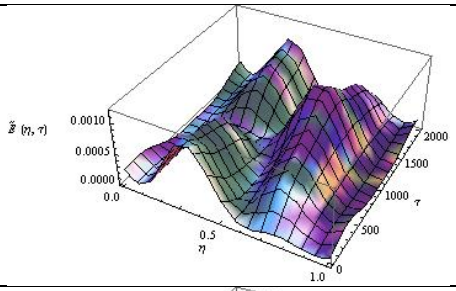
14 dof model	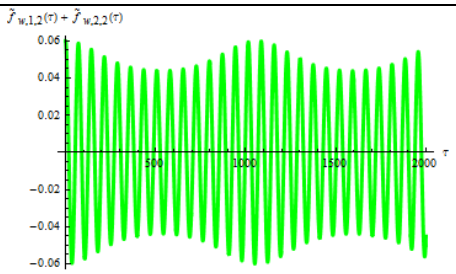	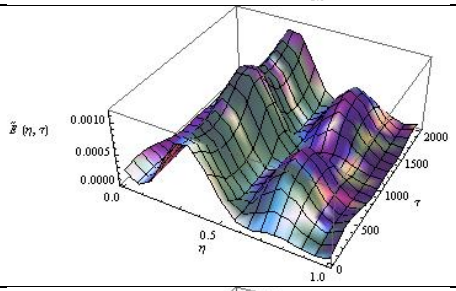
16 dof model	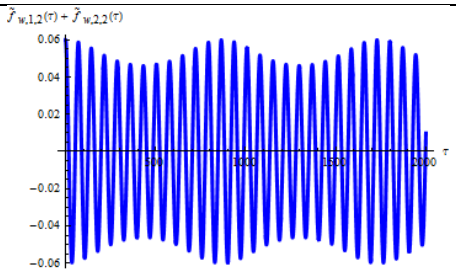	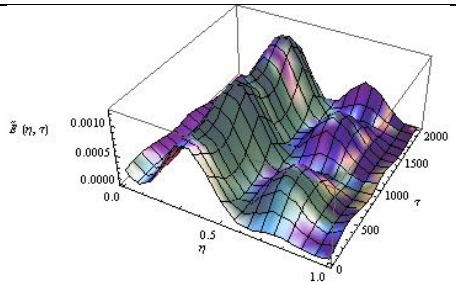
22 dof model	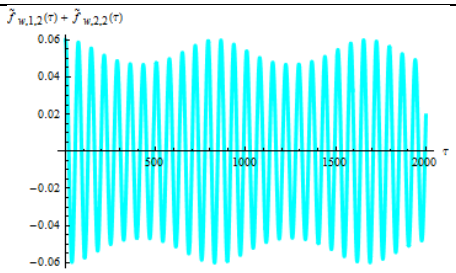	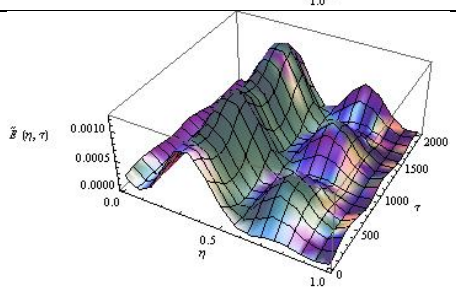
24 dof model	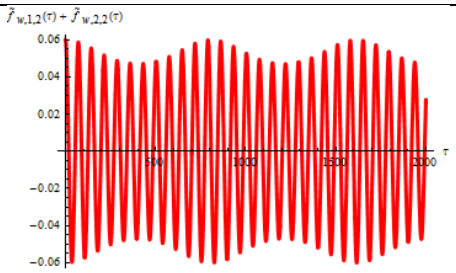	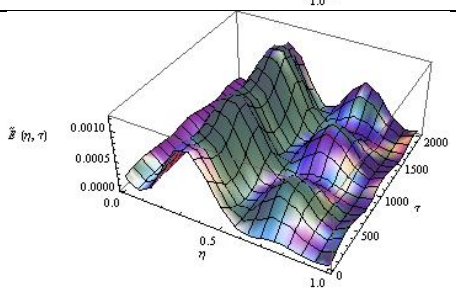
comparisons	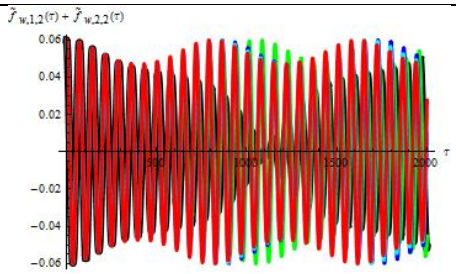	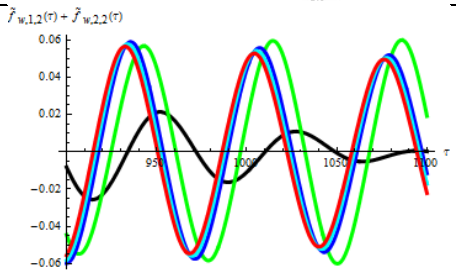

Figure 8. Convergence analysis. Numerical method. Nonlinear modal expansions (11). Clamped-clamped boundary conditions. Aspect ratio $L/R = 20$. $\tilde{X}(0) > \tilde{X}(0)_{\text{loc}}$ "—", 8 dof. "—", 14 dof. "—", 16 dof. "—", 22 dof. "—", 24 dof.

In Figures 9-10 and Tables 7-8, the convergence analysis for the numerical method in the case of free-free boundary conditions is reported. Time histories and energy distributions obtained by considering different expansions are compared for the aspect ratio L/R = 20. The corresponding energy localization threshold is $\tilde{X}(0)_{\text{loc}} = 0.07065$ and the modal expansion with 24 dof is assumed as the reference ($\text{ERROR}_{\text{RMS}}\% = 0$).

In Figure 9 and Table 7 the initial excitation amplitude $\tilde{X}(0) = 0.060$ is considered (lower than the threshold, $\tilde{X}(0) < \tilde{X}(0)_{\text{loc}}$). All models converge to a nonlinear behaviour very similar to the 24 dof model, with an energy beating.

In Figure 10 and Table 8 the initial excitation amplitude $\tilde{X}(0) = 0.080$ is considered (higher than the threshold, $\tilde{X}(0) > \tilde{X}(0)_{\text{loc}}$). The 8 dof model shows a nonlinear behaviour very different from the 24 dof one, with a wrong energy beating; conversely, the higher-order models from 14 to 22 dof converge to a nonlinear behaviour very similar to the 24 dof model, with an energy localization.

Similarly to the case of simply supported and clamped boundary conditions, it can be observed that, also in the case of free edges, the 16-22-24 dof expansions behave quite similarly and the smallest expansion able to predict the dynamics with acceptable accuracy is the 16 dof model ($\text{ERROR}_{\text{RMS}}\% \approx 5$).

(j,n)	(0,2)	(1,2)	(2,2)	(0,4)	(1,4)	(2,4)	(0,0)	(1,0)	(2,0)	$\text{ERROR}_{\text{RMS}}$%
8 dof model	*u*, *v*, *w*	*u*, *v*, *w*	–	–	–	–	*u*, *w*	–	–	12.42
14 dof model	*u*, *v*, *w*	*u*, *v*, *w*	–	*u*, *v*, *w*	*u*, *v*, *w*	–	*u*, *w*	–	–	8.37
16 dof model	***u*, *v*, *w***	***u*, *v*, *w***	**–**	***u*, *v*, *w***	***u*, *v*, *w***	**–**	***u*, *w***	***u*, *w***	**–**	**4.58**
22 dof model	*u*, *v*, *w*	*u*, *v*, *w*	*u*, *v*, *w*	*u*, *v*, *w*	*u*, *v*, *w*	*u*, *v*, *w*	*u*, *w*	*u*, *w*	–	1.78
24 dof model	*u*, *v*, *w*	*u*, *v*, *w*	*u*, *v*, *w*	*u*, *v*, *w*	*u*, *v*, *w*	*u*, *v*, *w*	*u*, *w*	*u*, *w*	*u*, *w*	

Table 7. Convergence analysis. Numerical method. Nonlinear modal expansions (11). $\text{ERROR}_{\text{RMS}}$% in time domain. 24 dof model reference. Free-free boundary conditions. Aspect ratio L/R = 20. Initial amplitude $\tilde{X}(0) < \tilde{X}(0)_{\text{loc}}$.

(j,n)	(0,2)	(1,2)	(2,2)	(0,4)	(1,4)	(2,4)	(0,0)	(1,0)	(2,0)	$\text{ERROR}_{\text{RMS}}$%
8 dof model	*u*, *v*, *w*	*u*, *v*, *w*	–	–	–	–	*u*, *w*	–	–	79.08
14 dof model	*u*, *v*, *w*	*u*, *v*, *w*	–	*u*, *v*, *w*	*u*, *v*, *w*	–	*u*, *w*	–	–	11.82
16 dof model	***u*, *v*, *w***	***u*, *v*, *w***	**–**	***u*, *v*, *w***	***u*, *v*, *w***	**–**	***u*, *w***	***u*, *w***	**–**	**5.40**
22 dof model	*u*, *v*, *w*	*u*, *v*, *w*	*u*, *v*, *w*	*u*, *v*, *w*	*u*, *v*, *w*	*u*, *v*, *w*	*u*, *w*	*u*, *w*	–	2.27
24 dof model	*u*, *v*, *w*	*u*, *v*, *w*	*u*, *v*, *w*	*u*, *v*, *w*	*u*, *v*, *w*	*u*, *v*, *w*	*u*, *w*	*u*, *w*	*u*, *w*	

Table 8. Convergence analysis. Numerical method. Nonlinear modal expansions (11). $\text{ERROR}_{\text{RMS}}$% in time domain. 24 dof model reference. Free-free boundary conditions. Aspect ratio L/R = 20. Initial amplitude $\tilde{X}(0) > \tilde{X}(0)_{\text{loc}}$.

Case	Time history	Energy distribution
8 dof model	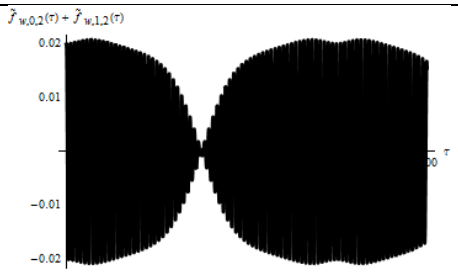	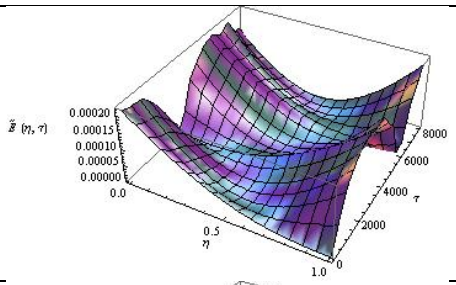
14 dof model	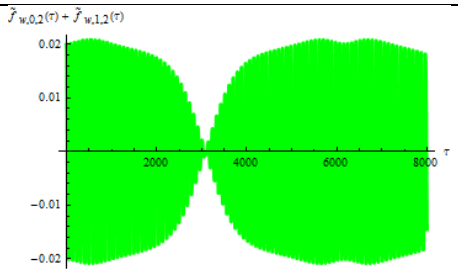	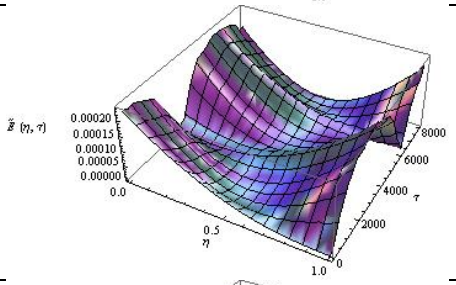
16 dof model	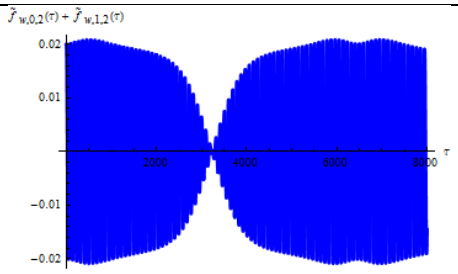	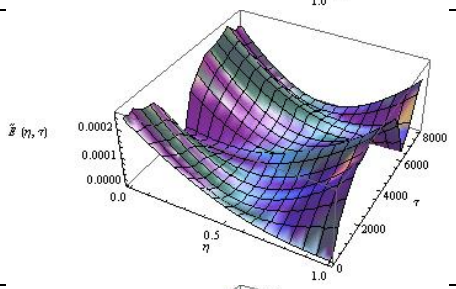
22 dof model	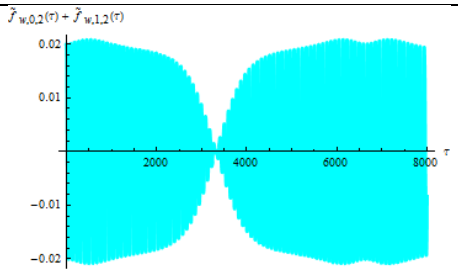	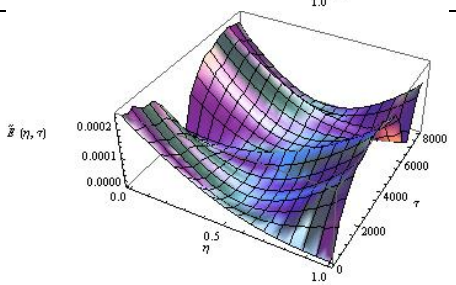
24 dof model	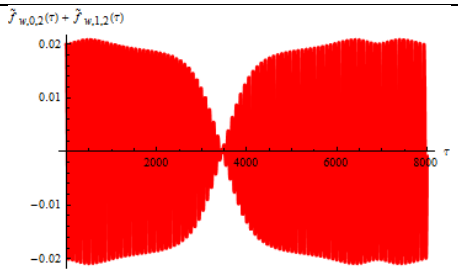	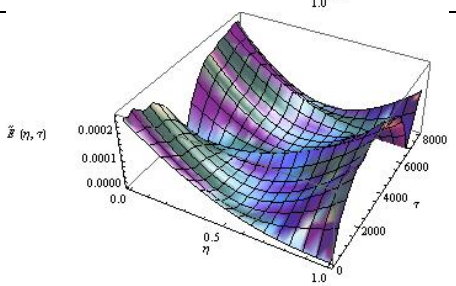
comparisons	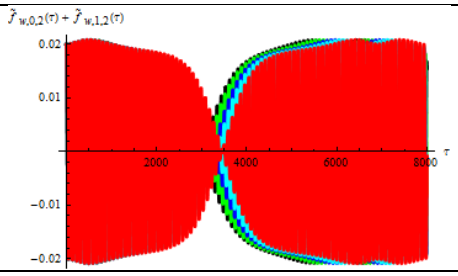	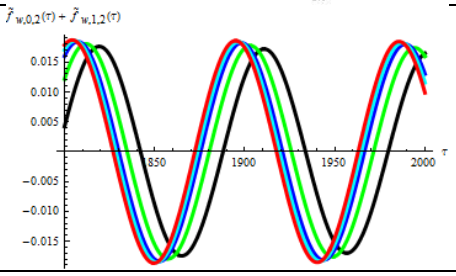

Figure 9. Convergence analysis. Numerical method. Nonlinear modal expansions (11). Free-free boundary conditions. Aspect ratio $L/R = 20$. $\tilde{X}(0) < \tilde{X}(0)_{\text{loc}}$ "—", 8 dof. "—", 14 dof. "—", 16 dof. "—", 22 dof. "—", 24 dof.

Case	Time history	Energy distribution
8 dof model	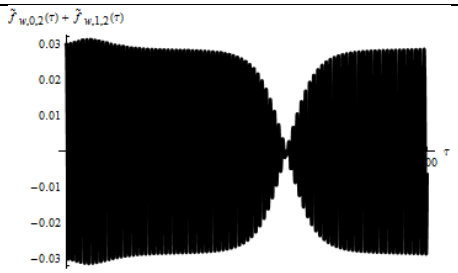	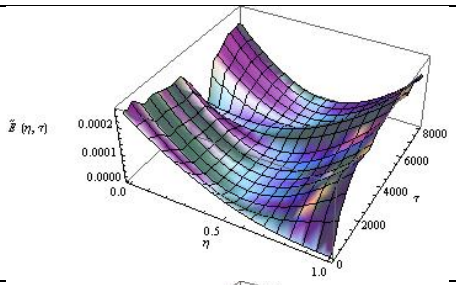
14 dof model	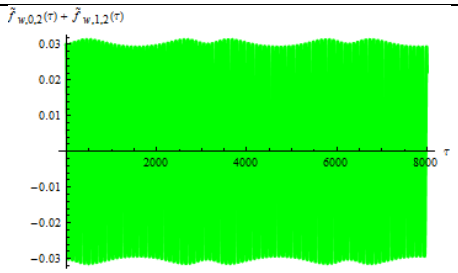	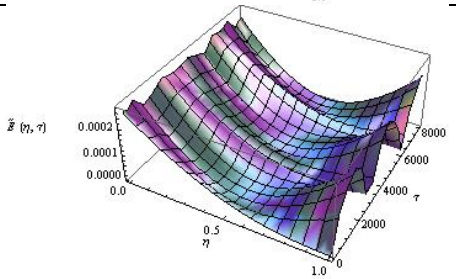
16 dof model	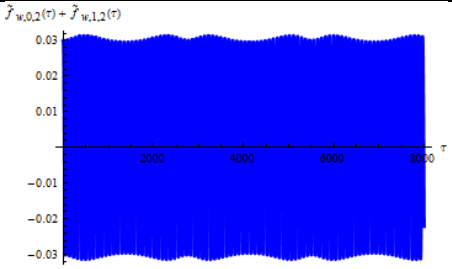	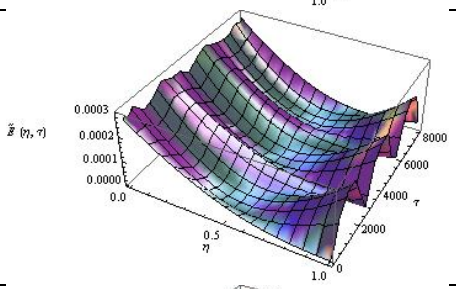
22 dof model	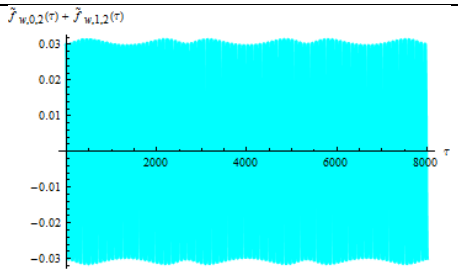	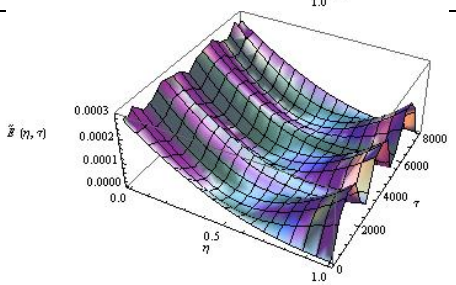
24 dof model	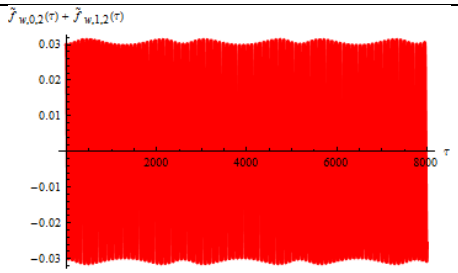	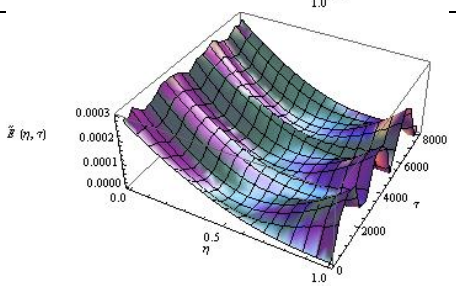
comparisons	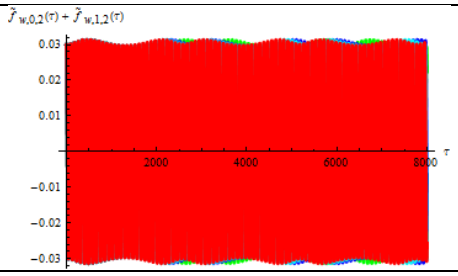	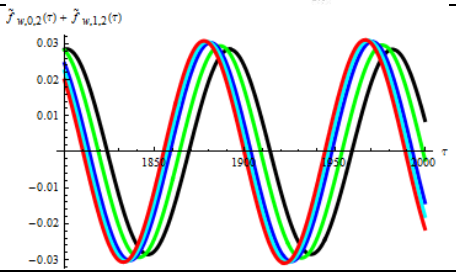

Figure 10. Convergence analysis. Numerical method. Nonlinear modal expansions (11). Free-free boundary conditions. Aspect ratio $L/R = 20$. $\tilde{X}(0) > \tilde{X}(0)_{\text{loc}}$ "—", 8 dof. "—", 14 dof. "—", 16 dof. "—", 22 dof. "—", 24 dof.

From all the three convergence analyses, it can be deduced that the 16 dof models (Tables 3-8) provide satisfactory results with minimal computational effort; therefore, in the following the 16 dof models of Figures 5-10 will be used.

The main result of the present convergence analysis is the following: using an insufficient modal expansion leads to a wrong nonlinear behaviour; in particular, the energy localization phenomenon can be lost.

The previous considerations suggest that the following 16 dof model should be used for studying the resonant circumferential flexural modes (j,n), (j+1,n):

- modes (j,n), (j+1,n), (j,2n), (j+1,2n), (j,0), (j+1,0) for the longitudinal displacement field u
- modes (j,n), (j+1,n), (j,2n), (j+1,2n) for the circumferential displacement field v
- modes (j,n), (j+1,n), (j,2n), (j+1,2n), (j,0), (j+1,0) for the radial displacement field w

with $j = 1$ in the case of simply supported and clamped-clamped SWNTs, $j = 0$ in the case of free-free SWNTs, and $n = 2$ (circumferential flexural modes).

After selecting these modes, the longitudinal and radial expansions of equations (11) are reduced to a six-term model, while the circumferential expansion is reduced to a four-term model; the resulting nonlinear system has therefore a total number of 16 dof.

6.2. Energy localization threshold

In this section, analytical and numerical estimations of the nonlinear energy localization threshold are compared for different boundary conditions. The comparisons are carried out in the specific interval of aspect ratios $\lambda = 20 \div 90$, since for the aspect ratios $\lambda < 20$ and $\lambda > 90$ the present analysis is not valid (the assumptions of the reduced Sanders-Koiter shell theory are not applicable, see Ref. [17] for more details).

In the case of simply supported boundary conditions (Figure 11), the correspondence between the analytical and numerical methods is very good for the whole interval of aspect ratios. A fast increment of the localization threshold in the lower region of aspect ratios $\lambda = 20 \div 40$ is found. The localization threshold increment is monotonic with L/R, reaching an horizontal asymptote at $\lambda \approx 70$.

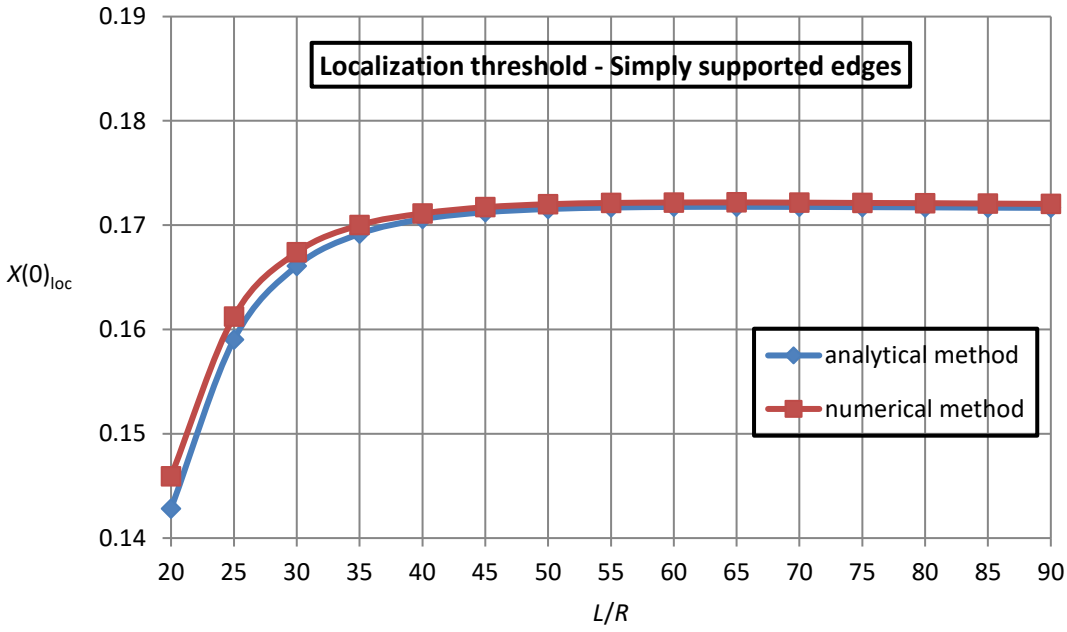

Figure 11. Effect of the aspect ratio on the amplitude of the localization threshold for the SWNT with simply supported boundary conditions of Table 1. "-♦-", analytical method (RSKT); "-■-", numerical method (CSKT).

In the case of clamped-clamped boundary conditions (Figure 12), the correspondence between the analytical and numerical methods is good for the whole interval of aspect ratios. The localization threshold increases with L/R up to $\lambda = 35$, where the frequency ratios $\omega_{3,2}/\omega_{1,2}$ and $\omega_{2,2}/\omega_{1,2}$ approach the unity ($\lambda = 30$: $\omega_{2,2}/\omega_{1,2} = 1.032$, $\omega_{3,2}/\omega_{1,2} = 1.118$; $\lambda = 40$: $\omega_{2,2}/\omega_{1,2} = 1.012$, $\omega_{3,2}/\omega_{1,2} = 1.044$) and a 1:1:1 weak internal resonance takes place. Then, there is a localization threshold decrement up to $\lambda = 40$, which is followed by a maximum of localization threshold at $\lambda \approx 50$, where the frequency ratios $\omega_{3,2}/\omega_{2,2}$ and $\omega_{2,2}/\omega_{1,2}$ approach the unity ($\lambda = 45$: $\omega_{2,2}/\omega_{1,2} = 1.009$, $\omega_{3,2}/\omega_{2,2} = 1.021$; $\lambda = 55$: $\omega_{2,2}/\omega_{1,2} = 1.004$, $\omega_{3,2}/\omega_{2,2} = 1.008$) and a 1:1:1 strong internal resonance takes place. The localization threshold decreases with L/R from $\lambda = 55$, achieving an horizontal asymptote at $\lambda \approx 80$.

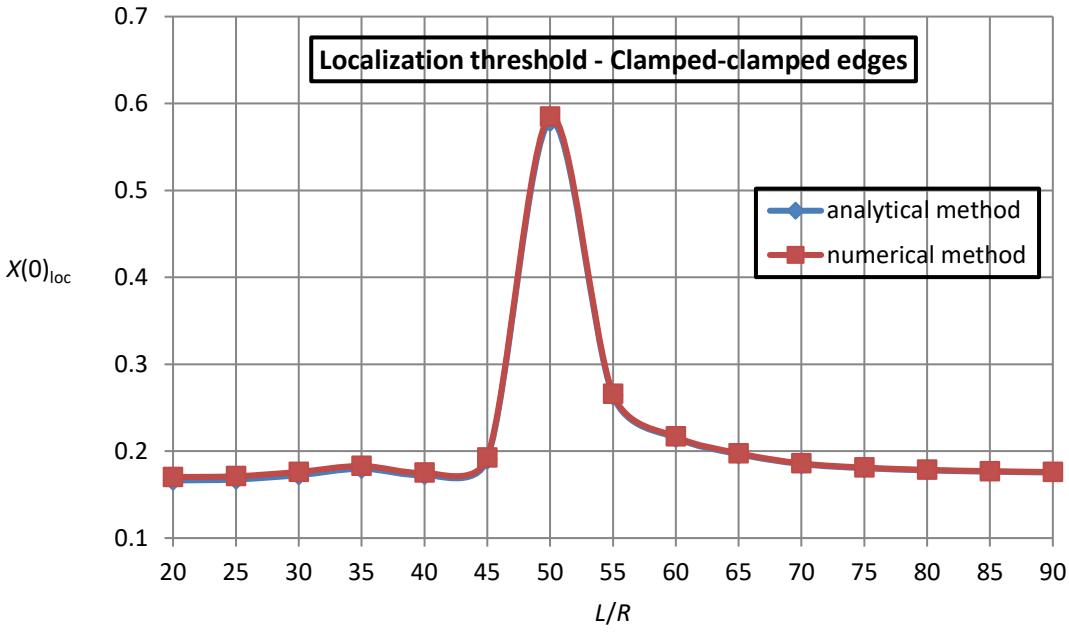

Figure 12. Effect of the aspect ratio on the amplitude of the localization threshold for the SWNT with clamped-clamped boundary conditions of Table 1. "-♦-", analytical method (RSKT); "-■-", numerical method (CSKT).

In the case of free-free boundary conditions (Figure 13), the correspondence between the analytical and numerical methods is good for the whole interval of aspect ratios. A very slow increment of the localization threshold in the lower region of aspect ratios λ = 20÷50 is found. A jump of the localization threshold is located at λ = 55, where the frequency ratios $\omega_{3,2}/\omega_{2,2}$ and $\omega_{2,2}/\omega_{1,2}$ approach the unity (λ = 50: $\omega_{2,2}/\omega_{1,2}$ = 1.0015, $\omega_{3,2}/\omega_{2,2}$ = 1.0061; λ = 60: $\omega_{2,2}/\omega_{1,2}$ = 1.0010, $\omega_{3,2}/\omega_{2,2}$ = 1.0036) and a 1:1:1 strong internal resonance takes place. The localization threshold increment is then monotonic with L/R.

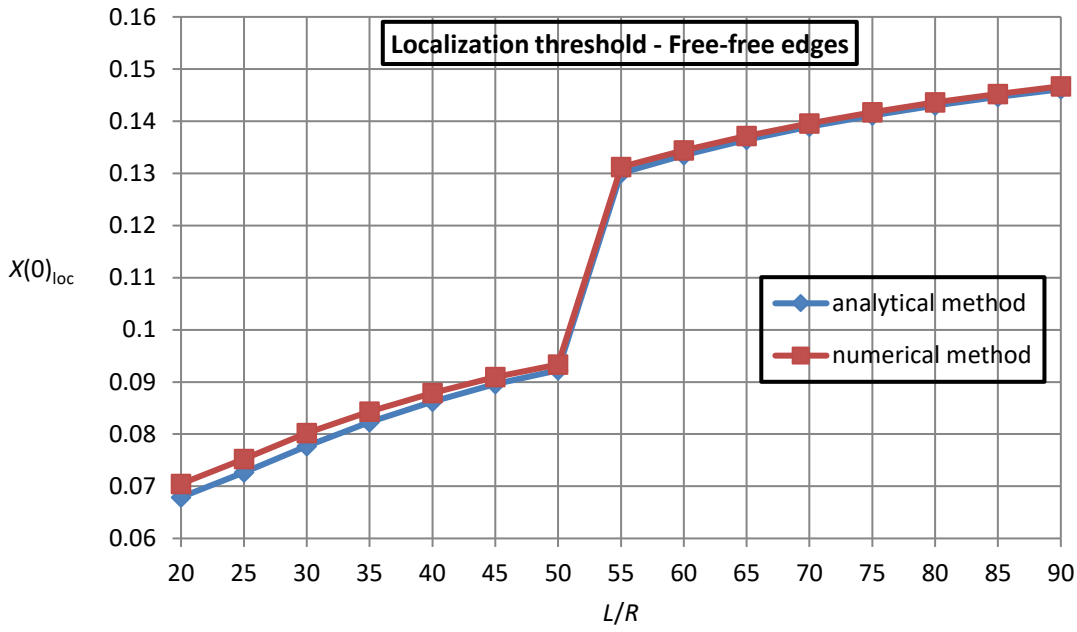

Figure 13. Effect of the aspect ratio on the amplitude of the localization threshold for the SWNT with free-free boundary conditions of Table 1. "-♦-", analytical method (RSKT); "-■-", numerical method (CSKT).

For all the boundary conditions, the results of the analytical and numerical methods are in perfect agreement for $\lambda \geq 70$, since the effect of the boundary conditions can be neglected far from the edges.

In the case of free-free boundary conditions, the value of the localization threshold at $\lambda = 90$, $X_{\text{loc}} \approx 0.146$, is lower than the corresponding value for the other two boundary conditions, $X_{\text{loc}} \approx 0.170$: in the free-free boundary conditions, the combination of resonant modes (0,2) and (1,2) is considered, where the uniform vibration mode (0,2) with $j = 0$ longitudinal half-waves loses its stability at a relatively low energy level; on the other hand, in the simply supported and clamped-clamped boundary conditions, the resonant modes (1,2) and (2,2) with $j = 1$ and $j = 2$ longitudinal half-waves are considered, which lose their stability at a relatively high energy level.

7. Conclusions

In this paper, the nonlinear vibrations and energy exchange of SWNTs are studied. The Sanders-Koiter theory is applied to model the nonlinear dynamics of the system. Simply supported, clamped and free boundary conditions are considered. The CFMs are analysed. Two different approaches are developed, based on numerical and analytical models. A nonlinear convergence analysis is carried out for the numerical method to select the correct number of axisymmetric and asymmetric modes providing the effective nonlinear behaviour of the SWNTs. For all the studied boundary conditions, an insufficient modal expansion leads to a wrong nonlinear behaviour. On the other hand, the 16 dof expansion containing four asymmetric and two axisymmetric modes describes the correct nonlinear behaviour with the minimal computational effort. In this nonlinear convergence analysis, it is well confirmed the fundamental role of the higher-order asymmetric and axisymmetric modes for properly modelling the bending deformation and circumferential stretching of the mode vibration. The influence of the aspect ratio on the analytical and numerical values of the energy localization threshold is investigated in nonlinear field. For all the considered boundary conditions, the results of the analytical and numerical methods almost coincide at the high aspect ratios, since the boundary conditions effect can be neglected far from the edges. Moreover, a good correspondence between the results of the two approaches is found for the intermediate interval of the aspect ratios, where a maximum of the localization threshold in the case of clamped edges and a jump of the localization threshold in the case of free edges take place, which are related to internal resonances. Eventually, for the free boundary conditions the energy localization threshold at high aspect ratios is lower than the correspondent value for the other boundary conditions; indeed, in the case of free-free edges the uniform vibrational mode presenting zero longitudinal half-waves loses its stability at relatively low energy level. The present paper, which is devoted to the CFMs, could represent a framework also in the study of the nonlinear vibrations and energy exchange of the beam-like modes (BLMs) and the radial breathing (axisymmetric) modes (RBMs).

References

[1] Manevitch L.I., Gendelman O.V. *Tractable Models of Solid Mechanics. Formulation, Analysis and Interpretation*. Springer-Verlag, Berlin, 2011.

[2] Balandin D.V., Bolotnik N.N., Pilkey W.D. *Optimal Protection From Impact, Shock, and Vibration*. Overseas Publishers Association, Amsterdam, 2001.

[3] Scott A. *Nonlinear Science: Emergence and Dynamics of Coherent Structures*. Oxford University Press, New York, 2003.

[4] Manevitch L.I., Musienko A.I. Limiting phase trajectories and energy exchange between anharmonic oscillator and external force. *Nonlinear Dynamics* 58 (2009) 633-642.

[5] Manevitch L.I., Kovaleva A.S., Manevitch E.L. Limiting phase trajectories and energy transfer in a system of two coupled oscillators. *Mathematical Problems in Engineering* 2010 (2010) 1-24.

[6] Manevitch L.I., Smirnov V.V. Limiting phase trajectories and the origin of energy localization in nonlinear oscillatory chains. *Physical Review E* 82 (2010) 1-9.

[7] Smirnov V.V., Manevitch L.I. Limiting Phase Trajectories and Dynamic Transitions in Nonlinear Periodic Systems. *Acoustical Physics* 57 (2011) 271-276.

[8] Iijima S. Helical microtubules of graphitic carbon. *Nature* 354 (1991) 56-58.

[9] Smirnov V.V., Shepelev D.S., Manevitch L.I. Localization of bending vibrations in the Single-Wall Carbon Nanotubes. *Nanosystems: Physics, Chemistry, Mathematics* 2 (2011) 102-106.

[10] Smirnov V.V., Manevitch L.I., Strozzi M., Pellicano F. Nonlinear optical vibrations of single-walled carbon nanotubes. 1. Energy exchange and localization of low-frequency oscillations. *Physica D* 325 (2016) 113-125.

[11] Y.Y. Zhang, C.M. Wang, V.B.C. Tan. Assessment of Timoshenko Beam Models for Vibrational Behaviour of Single-Walled Carbon Nanotubes using Molecular Dynamics. *Advances in Applied Mathematics and Mechanics* 1 (2009) 89-106.

[12] Liew K.M., Wang Q. Analysis of wave propagation in carbon nanotubes via elastic shell theories. *International Journal of Engineering Science* 45 (2007) 227-241.

[13] Wang C.Y., Ru C.Q., Mioduchowski A. Applicability and Limitations of Simplified Elastic Shell Equations for Carbon Nanotubes. *Journal of Applied Mechanics* 71 (2004) 622-631.

[14] Silvestre N. On the accuracy of shell models for torsional buckling of carbon nanotubes. *European Journal of Mechanics A/Solids* 32 (2012) 103-108.

[15] Hu Y.G., Liew K.M., Wang Q., He X.Q., Yacobson B.I. Nonlocal shell model for elastic wave propagation in single and double-walled carbon nanotubes. *Journal of the Mechanics and Physics of Solids* 56 (2008) 3475-3485.

[16] Silvestre N., Wang C.M., Zhang Y.Y., Xiang Y. Sanders shell model for buckling of single-walled carbon nanotubes with small aspect ratio. *Composite Structures* 93 (2011) 1683-1691.

[17] Strozzi M., Manevitch L.I., Pellicano F., Smirnov V.V., Shepelev D.S. Low-frequency linear vibrations of single-walled carbon nanotubes: Analytical and numerical models. *Journal of Sound and Vibration* 333 (2014) 2936-2957.

[18] Zhen Y.X., Fang B. Nonlinear vibration of fluid-conveying single-walled carbon nanotubes under harmonic excitation. *International Journal of Non-Linear Mechanics* 76 (2015) 48-55.

[19] Ansari R., Arash B. Nonlocal Flugge Shell Model for Vibrations of Double-Walled Carbon Nanotubes With Different Boundary Conditions. *Journal of Applied Mechanics* 80 (2013) 021006.

[20] Ansari R., Shahabodini A., Rouhi H. A thickness-independent nonlocal shell model for describing the stability behavior of carbon nanotubes under compression. *Composite Structures* 100 (2013) 323-331.

[21] Ansari R., Gholami R., Rouhi H. Various gradient elasticity theories in predicting vibrational response of single-walled carbon nanotubes with arbitrary boundary conditions. *Journal of Vibration and Control* 19 (2013) 708-719.

[22] Cigeroglu E., Samandari H. Nonlinear free vibrations of curved double walled carbon nanotubes using differential quadrature method. *Physica E* 64 (2014) 95-105.

[23] Ansari R., Rouhi H., Mirnezhad M. A hybrid continuum and molecular mechanics model for the axial buckling of chiral single-walled carbon nanotubes. *Current Applied Physics* 14 (2014) 1360-1368.

[24] Ansari R., Arjangpay A. Nanoscale vibration and buckling of single-walled carbon nanotubes using the meshless local Petrov-Galerkin method. *Physica E* 63 (2014) 283-292.

[25] Ansari R., Norouzzadeh A., Gholami R., Faghih Shojaei M., Hosseinzadeh M. Size-dependent nonlinear vibration and instability of embedded fluid-conveying SWBNNTs in thermal environment. *Physica E* 61 (2014) 148-157.

[26] Khosrozadeh A., Hajabasi M.A. Free vibration of embedded double-walled carbon nanotubes considering nonlinear interlayer van der Waals forces. *Applied Mathematical Modelling* 36 (2012) 997-1007.

[27] Ansari R., Rouhi H., Sahmani S. Free vibration analysis of single- and double-walled carbon nanotubes based on nonlocal elastic shell models. *Journal of Vibration and Control* 20 (2014) 670-678.

[28] Rouhi H., Ansari R., Darvizeh M. Size-dependent free vibration analysis of nanoshells based on the surface stress elasticity. *Applied Mathematical Modelling* 40 (2016) 3128-3140.

[29] Leissa A.W. *Vibrations of Shells*. Government Printing Office, Washington DC, 1973.

[30] Yamaki N. *Elastic Stability of Circular Cylindrical Shells*. North-Holland, Amsterdam, 1984.

[31] Amabili M. *Nonlinear Vibrations and Stability of Shells and Plates*. Cambridge University Press, New York, 2008.

[32] Amabili M. A comparison of shell theories for large-amplitude vibration of circular cylindrical shells: Lagrangian approach. *Journal of Sound and Vibration* 264 (2003) 1091-1125.

[33] Kurylov Y., Amabili M. Nonlinear vibrations of clamped-free circular cylindrical shells. *Journal of Sound and Vibration* 330 (2011) 5363-5381.

[34] Pellicano F. Vibrations of circular cylindrical shells: Theory and experiments. *Journal of Sound and Vibration* 303 (2007) 154-170.

[35] Amabili M. Nonlinear Vibrations of Circular Cylindrical Shells with Different Boundary Conditions. *American Institute of Aeronautics and Astronautics Journal* 41 (2003) 1119-1130.

[36] Zhang L., Xiang Y., Wei G. Local adaptive differential quadrature for free vibration analysis of cylindrical shells with various boundary conditions. *International Journal of Mechanical Sciences* 48 (2006) 1126-1138.

[37] Kurylov Y., Amabili M. Polynomial versus trigonometric expansions for nonlinear vibrations of circular cylindrical shells with different boundary conditions. *Journal of Sound and Vibration* 329 (2010) 1435-1449.

[38] Strozzi M., Pellicano F. Nonlinear vibrations of functionally graded cylindrical shells. *Thin-Walled Structures* 67 (2013) 63-77.

[39] Pellicano F., Barbieri M., Zippo A., Strozzi M. Experiments on shells under base excitation. *Journal of Sound and Vibration* 369 (2016) 209-227.

[40] Pellicano F., Barbieri M. Complex dynamics of circular cylindrical shells. *International Journal of Non-Linear Mechanics* 65 (2014) 196-212.